RESEARCH/REVIEW ARTICLE

# An inter-comparison of six latent and sensible heat flux products over the Southern Ocean

Lejiang Yu,[1,2] Zhanhai Zhang,[2] Shiyuan Zhong,[3] Mingyu Zhou,[2] Zhiqiu Gao,[4] Huiding Wu[2] & Bo Sun[2]

[1] Applied Hydrometeorological Research Institute, Nanjing University of Information Science & Technology, Nanjing 210044, China
[2] Polar Research Institute of China, 451 Jinqiao Road, Pu Dong, Shanghai 200136, China
[3] Department of Geography, 208 Geography Building, Michigan State University East Lansing, MI 48824, USA
[4] Institute of Atmospheric Physics, Chinese Academy of Sciences, Beijing 100029, China

**Keywords**
Latent heat flux; sensible heat flux; Southern Ocean.

**Correspondence**
Lejiang Yu, Applied Hydrometeorological Research Institute, Nanjing University of Information Science & Technology, 219 Ningliu Road, Nanjing, 210044, China.
E-mail: yulejiang@sina.com.cn

## Abstract

The latent heat fluxes (LHF) and sensible heat fluxes (SHF) over the Southern Ocean from six different data sets are inter-compared for the period 1988–2000. The six data sets include three satellite-based products, namely, the second version of the Goddard Satellite-Based Surface Turbulent Fluxes data set (GSSTF-2), the third version of the Hamburg Ocean Atmosphere Parameters and Fluxes from Satellite Data (HOAPS-3) and the Japanese Ocean Fluxes Data Sets with Use of Remote Sensing Observations (J-OFURO); two global reanalysis products, namely, the National Centers for Environmental Prediction–Department of Energy Reanalysis 2 data set (NCEP-2) and the European Centre for Medium-Range Weather Forecasts 40 Year Re-analysis data set (ERA-40); and the Objectively Analyzed Air–Sea Fluxes for the Global Oceans data set (OAFlux). All these products reveal a similar pattern in the averaged flux fields. The zonal mean LHF fields all exhibit a continuous increase equatorward. With an exception of HOAPS-3, the zonal mean SHF fields display a minimum value near 50°S, increasing both pole- and equatorward. The differences in the standard deviation for LHF are larger among the six data products than the differences for SHF. Over the regions where the surface fluxes are significantly influenced by the Antarctic Oscillation and the Pacific–South American teleconnection, the values and distributions of both LHF and SHF are consistent among the six products. It was found that the spatial patterns of the standard deviations and trends of LHF and SHF can be explained primarily by sea–air specific humidity and temperature differences; wind speed plays a minor role.

The Southern Ocean plays an important role in the variability of weather and climate at southern high latitudes through heat and moisture transfer between the upper ocean and the atmospheric boundary layer (King & Turner 1997; Li et al. 1997). Monitoring heat transfer between the ocean and the atmosphere is therefore crucial for understanding the climate system at southern high latitudes. The components of atmospheric–ocean heat transfer include short- and long-wave radiative fluxes and latent heat fluxes (LHF) and sensible heat fluxes (SHF). Because LHF and SHF have large inter-annual and spatial variability (Josey et al. 1999; Chou et al. 2004) it is especially important to observe and obtain a reliable long-term estimate of these fluxes over the Southern Ocean.

Recognizing the importance of LHF and SHF in atmospheric circulation and weather and climate modelling has led to the construction of several recent flux data sets from a variety of sources. Some, such as that of da Silva et al. (1994), come from observational data. Satellite-derived data sets include the third version of the Hamburg Ocean Atmosphere Parameters and Fluxes


Citation: *Polar Research* 2011, *30*, 10167, DOI: 10.3402/polar.v30i0.10167

from Satellite Data (HOAPS-3; Andersson et al. 2007), the second version of the Goddard Satellite-Based Surface Turbulent Fluxes data set (GSSTF-2; Chou et al. 1997; Chou et al. 2000; Chou et al. 2003) and the Japanese Ocean Fluxes Data Sets with Use of Remote Sensing Observations data set (J-OFURO; Kubota et al. 2002). There are also re-analysis products such as the National Centers for Environmental Prediction Reanalysis 2 data set (NCEP-2; Kanamitsu et al. 2002) and the European Centre for Medium-Range Weather Forecasts 40 Year Re-analysis (ERA-40; Uppala et al. 2005). Finally, there are products that comprise a mix of observation and reanalysis data such as the Objectively Analyzed Air–Sea Fluxes for the Global Oceans data set (OAFlux; Yu & Weller 2007). The World Climate Research Programme's Global Energy and Water Cycle Experiment Radiation Panel has established a sea surface turbulent flux project called SEAFLUX (Curry et al. 2004), and the project website contains various flux data sets, including those described above for inter-comparison studies and other research purposes.

Several studies have examined the behaviours of these flux data sets and earlier versions of them. Chou et al. (2003) compared the zonal averages of the GSSTF-2 LHF and the input parameters used in the bulk parameterizations over global oceans with those of HOAPS-2, National Centers for Environmental Prediction Reanalysis 2 (NCEP-2) and da Silva et al.'s (1994) data sets for the 2-year mean of 1992–1993 and found that GSSTF-2 LHF and bulk parameters differ significantly from those in these other data sets. In a further analysis, Chou et al. (2004) indicated that GSSTF-2 LHF, surface air humidity and winds are more realistic than those in HOAPS-3, NCEP-2 and da Silva et al.'s (1994) data sets during 1992–1993, although those in GSSTF-2 are still subject to regional biases. Wang & McPhaden (2001) compared six state-of-the-art surface heat flux products (tuned Da Silva, untuned Da Silva, the data from the Southampton Oceanography Centre, NCEP-2, ERA-40 and the data from the Goddard Earth Observing System data assimilation system) with the heat fluxes computed from Tropical Atmosphere–Ocean buoy data and found that these products show large deviations from Tropical Atmosphere–Ocean buoy data. Feng & Li (2006) compared the ERA-40 and NCEP-2 monthly LHF data with GSSTF-2 from 1988 to 2000 over the global oceans between 60°S and 60°N and found that the annual mean LHF in NCEP-2 is closer to GSSTF-2 than that in ERA-40 at high latitudes. Liu & Curry (2006) assessed the inter-annual variability and decadal trend of the ocean surface LHF among GSSTF-2, HOAPS-2, NCEP-2 and ERA-40 from 1989 to 2000 over the tropics and subtropics and found relatively good agreement in the spatial/temporal variations of the LHF; they attributed the discrepancies mainly to air-specific humidity. Kubota et al. (2003) compared LHF in J-OFURO with those in HOAPS-3, GSSTF-2, ERA-40 and NCEP-2 and da Silva et al.'s (1994) fields from 1992 to 1994. Their study found that all products qualitatively reveal a similar pattern in the average fields, but the temporal correlation between J-OFURO and da Silva et al.'s data set (1994) is low in the Southern Hemisphere, and because of the lack of ship observations, the time correlation between J-OFURO and ERA-40 or NCEP-1 is considerably lower in the Southern Hemisphere than in the Northern Hemisphere.

Although in situ observations over ocean surfaces are sparse compared to land surface observations, some buoy and ship observations are available for comparison. Josey (2001) compared re-analysis data with ocean surface observations made by buoys and indicated that NCEP-2 and ERA-40 re-analyses underestimate the ocean heat gain in the north-east Atlantic. Rouault et al. (2003) showed that over the waters of the Agulhas Current, LHF and SHF are also underestimated by NCEP-2 and ERA-40. Over regions with large air–sea temperature difference and high wind speed, such as the Labrador Sea, the Norwegian Sea, the Gulf Stream and the Kuroshio Current, the ERA-40 surface LHF and SHF compare reasonably well with observations than those in NCEP-2 (Moore & Renfrew 2002; Renfrew et al. 2002; Bentamy et al. 2003). Over the Kuroshio Extension region, J-OFURO-2 air–sea heat fluxes are found to be better than NCEP-2, Hamburg Ocean Atmosphere Parameters and Fluxes from Satellite Data (HOAPS-3 and OAFlux (Tomita et al. 2010). Bentamy et al. (2003) compared weekly satellite flux estimates to surface data derived from moored buoys in three areas during nine months (October 1996 to June 1997). They found that the accuracy of their LHF estimates was within 30 W $m^{-2}$. Comparing HOAPS-2, J-OFURO, GSSTF-2, the Jones data set and the Bourras–Eymard–Liu data set LHF with data from 75 moored buoys, Bourras (2006) concluded that HOAPS-2 is the most appropriate product for applications of the satellite fluxes to the world oceans.

The differences among data sets may result from the differences in the bulk aerodynamic algorithms used to derive the flux values. Brunke and co-workers (Brunke et al. 2002; Brunke et al. 2003) evaluated and ranked 12 such algorithms and recommended four least problematic algorithms: version 3 of the Coupled Ocean–Atmosphere Response Experiment (COARE); the University of Arizona schemes; those used at the European Centre



Citation: *Polar Research* 2011, *30*, 10167, DOI: 10.3402/polar.v30i0.10167

for Medium-Range Weather Forecasts (ECMWF); and the National Aeronautics and Space Administration (NASA) Data Assimilation System for version 1 of the Goddard Earth Observing System reanalysis.

These previous studies have provided us with very useful information about the behaviour of surface heat fluxes and input parameters in various satellite and re-analysis products over regions of global ocean. However, the comparison or inter-comparison studies to date are limited to either short periods (<5 years) or smaller numbers of data sets (<4 members). In addition, few studies have focused specifically on the Southern Ocean.

The current article describes an inter-comparison of monthly LHF and SHF over the Southern Ocean from six different gridded data sets, including three satellite-derived products (GSSTF-2, HOAPS-3 and J-OFURO), one objectively analysis data set (OAFlux) and two re-analysis data sets (NCEP-2 and ERA-40). The time span examined is the 13-year period of 1988–2000, when all six data sets overlap. Although many validation or intercomparison studies have focused on LHF over ocean surfaces, little attention has been given to the SHF. This is partially because of the dominancy of LHF over SHF over ocean surfaces. The current study examines both SHF and LHF values over the Southern Ocean.

The data sets are briefly described in the following sections. The subsequent two sections present the inter-comparison results and discuss the impact of wind, specific humidity and temperature on the difference of LHF and SHF. Conclusions are drawn in the final section of the article.

## Data sets

Measurements of turbulent LHF and SHF are difficult to obtain, especially over ocean surfaces. As a result, the heat fluxes are usually derived using some types of a bulk parameterization based on differences of mean temperature, specific humidity and wind speed between ocean surfaces and the atmospheric layer immediately above. Drawing from Curry & Webster (1999) Curry & Webster (1999a) typical form of bulk parameterization can be written as:

$$S_E = \rho c_P C_S (U_A - U_0)(T_S - T_A),$$
$$L_E = \rho L_V C_L (U_A - U_0)(Q_S - Q_A),$$

where $S_E$ and $L_E$ are SHF and LHF, respectively; ρ is air density; $c_P$ is the constant-pressure specific heat; $L_V$ is the latent heat of vaporization; $C_S$ and $C_L$ are the aerodynamic transfer coefficients for temperature and humidity, which under ordinary conditions are nearly equal and depend partly on the ocean surface roughness length and the bulk Richardson number. $T_S$ is sea surface temperature (SST) and $T_A$ and $Q_A$ are the air temperature and the specific humidity at an atmospheric reference level that is typically 2 m; $Q_S$ is the specific humidity at the sea surface and is assumed to be 98% of the saturation humidity at the SST. $U_A$ is the wind speed at 10 m and $U_0$ is ocean surface velocity along the wind direction, which is commonly neglected except in regions of the ocean with strong surface currents and weak winds over it such as in the tropics and in the Kuroshio Current system (Dawe & Thompson 2006).

## Goddard satellite-based surface turbulent fluxes data set

The GSSTF-2 data set provides 1° latitude by 1° longitude gridded global ocean monthly mean, values of surface fluxes from July 1987 to December 2000. The fluxes are derived using a bulk parameterization scheme (Chou 1993). Air temperatures and SST needed by the parameterization are from NCEP-2, whereas surface wind speed and air specific humidity are derived from the Special Sensor Microwave/Imager (SSM/I) using the algorithms of Wentz (1997) and Chou et al. (1997), respectively. Chou et al. (2003) indicated that the LHF in the GSSTF-2 data set are more realistic than those in HOAPS-3, NCEP-2 and the Comprehensive Ocean–Atmosphere Data Set (COADS). For a more detailed description of GSSTF-2 and its comparison with other data sets, refer to Chou et al. (2003). Compared to the GSSTF-1, the GSSTF-2 involves two improvements. The first improvement is related to the salinity effect on the saturation-specific humidity at the sea surface, whereas the GSSTF-1 ignores this effect. The second improvement is related to the assumptions of the von Karman constants. The GSSTF-1 model chooses different von Karman constants of 0.4, 0.36 and 0.45, for velocity, temperature and humidity, respectively. On the other hand, the GSSTF-2 model assumes the same von Karman constant of 0.4 for the three variables, in close agreement with observations (Zeng et al. 1998; Brunke et al. 2003). Hence, the outdated version of GSSTF-2 is used in this study.

## Hamburg ocean atmosphere parameters and fluxes from satellite

The HOAPS-3 data set supplies global ocean fields of LHF and SHF with a spatial resolution of 0.5 degrees from January 1987 to December 2005 (Andersson et al. 2007). The most recent version includes a new neural network-based precipitation algorithm and utilizes the National Oceanographic Data Center/University

of Miami Rosenstiel School of Marine and Atmospheric Science Pathfinder version 5 SST data set and a new algorithm to synthesize the defective 85 GHz channel on the Defense Meteorological Satellite Program's F08 spacecraft. The heat fluxes, LHF and SHF, are estimated with the bulk aerodynamic approach (Fairall et al. 1996; Fairall et al. 2003). The wind speed ($U_A$) and specific humidity ($Q_A$) are inferred from the SSM/I and air temperature ($T_A$) is assumed to be from an averaged of two estimates: one of an assumed relative humidity and inversion of the Magnus (vapour pressure) formula given the SSM/I retrieved specific humidity, and a value given by the SST minus 1 degree (Bourras 2006). Klepp et al. (2008) revealed that the HOAPS-3 LHF climatology agrees reasonably well with the LHF climatology from several other data sets, including J-OFURO, GSSTF2, the data set of the Institut Francais pour la Recherche et l' Exploitation de la Mer, OAFlux and the data set of the National Oceanography Centre.

### Japanese ocean fluxes data sets with use of remote sensing observations

The J-OFURO data set offers global ocean fields of LHF and SHF with a spatial resolution of 1° latitude by 1° longitude from January 1987 to December 2005 (Kubota et al. 2002). The fluxes are obtained based on version 3 of the COARE bulk algorithm (Fairall et al. 2003), a modification of the earlier bulk algorithm proposed by Kondo (1975). The input parameter $Q_A$ is derived based on SSM/I (Wentz 1994), $U_A$ is estimated using all available satellite data (Kubota & Tomita 2007) and SST is derived from NCEP-2. The source of air temperature is NCEP-2. Here, J-OFURO-2 data set is used to compare other products.

### Objectively analysed air–sea fluxes for the global oceans

The OAFlux data set provides global ocean fields of LHF and SHF with a spatial resolution of 1° latitude by 1° longitude from January 1958 to December 2008 (Yu & Weller 2007). To obtain the best possible global daily estimates for $U_A$, $T_S$, $T_A$ and $Q_A$, the OAFlux synthesis uses surface meteorological fields derived from satellite remote sensing and re-analysis outputs produced from the NCEP and ECMWF models as well as an advanced objective analysis (Yu et al. 2008). Specific humidity is from both NCEP-2 and ERA-40 and SSM/I data. Surface air temperature comes from NCEP-2 and ERA-40 because satellite sensors have technical difficulties in retrieving air temperature at a few metres above the sea surface. The OAFlux project estimates surface air temperature using an advanced objective analysis. The fluxes are based on version 3 of the state-of-the-art COARE bulk flux algorithm to compute the fluxes.

### National Centers for Environmental Prediction Reanalysis 2

Described in detail by Kanamitsu et al. (2002), NCEP-2 updates and corrects known errors in NCEP-1. The two data sets differ largely in the parameterizations of short-wave radiation, cloud and soil moisture (Kanamitsu 1989; Kalnay et al. 1996; Kanamitsu et al. 2000). The NCEP-2 data set provides global fields of LHF and SHF with a spatial resolution of 1.9° latitude by 1.875° longitude from January 1979 to December 2009 (Kanamitsu et al. 2002). By comparing the turbulent fluxes and flux-related variables in NCEP-2 with measurements from moored buoys in the Atlantic Ocean, Sun et al. (2003) showed that, overall, NCEP-2 better estimates turbulent heat fluxes and fluxes-related variables compared to NCEP-1.

### European Centre for Medium-Range Weather Forecasts 40 Year Re-analysis

The ERA-40 data set contains global fields of LHF and SHF with a spatial resolution of $2.5° \times 2.5°$ for the period from September 1957 to August 2002 (Uppala et al. 2005). Through updating model parameterization and data assimilation schemes, ERA-40 obtains the up-to-date parameterizations of air–sea fluxes (Beljaars 1997; Klinker 1997). The change in the moisture transfer coefficients in 1990 for low wind speed and in 1993 for high wind speed brought the LHF up by about 20 W $m^{-2}$ in the equatorial region (Siefridt et al. 1999). The change in the sources of temperature and humidity profiles also had a considerable impact on the surface fluxes in the tropics (ECMWF 1994).

Table 1 provides a summary of these six data sets. The data sets differ in spatial and temporal resolution. Prior to inter-comparison, all data were transformed into a monthly mean data on a $1 \times 1$ grid.

## Results

### Annual mean and seasonal cycle

The differences in the annual means of LHF and SHF among the six data sets are first examined. Figure 1 shows the annual mean LHF calculated from the six data sets. Despite the differences in the values of LHF, all six data sets exhibit



Citation: *Polar Research* 2011, *30*, 10167, DOI: 10.3402/polar.v30i0.10167

**Table 1** Overview of the six data sets compared in this study: the second version of the Goddard Satellite-Based Surface Turbulent Fluxes (GSSTF-2), the third version of the Hamburg Ocean Atmosphere Parameters and Fluxes from Satellite Data (HOAPS-3), Japanese Ocean Fluxes Data Sets with Use of Remote Sensing Observations (J-OFURO), Objectively Analyzed Air–Sea Fluxes for the Global Oceans (OAFlux), National Centers for Environmental Prediction Reanalysis 2 (NCEP-2) and the European Centre for Medium-Range Weather Forecasts 40 Year Re-analysis (ERA-40).

| | GSSTF-2 | HOAPS-3 | J-OFURO | OAFlux | NCEP-2 | ERA-40 |
|---|---|---|---|---|---|---|
| Time extent | 7/87–12/00 | 7/87–12/05 | 1/88–12/06 | 1/58–12/08 | 1/79–present | 9/57–8/02 |
| Spatial sampling | 1 ×1 | 0.5 ×0.5° | 1 ×1° | 1 ×1 | 2.5 ×2.5° | 2.5 ×2.5° |
| Sea surface temperature | NCEP[a] | National Oceanographic Data Centre/ Rosenstiel School of Marine and Atmospheric Science Pathfinder V5 | NCEP[a] and Metop global data | National Oceanic and Atmospheric Administration Optimum, Interpolation and numerical weather prediction models | | |
| Specific humidity | SSM/I[b] (Chou et al. 1997) | SSM/I[b] (Bentamy et al. 2003) | SSM/I[b] (Schlussel et al. 1995) | Satellites and numerical weather prediction models | | |
| Wind speed | SSM/I[b] (Wentz 1997) | SSM/I[b] | SSM/I[b], European Remote-Sensing Satellite 1/2, QuikSCAT, MSR-E[c] and Tropical Rainfall Measuring Mission Microwave Imager (Kubota & Tomita 2007) | SSM/I[b], AMSR-E[c], Quick Scatterometer satellite and numerical weather prediction models (Yu et al. 2008) | | |
| Air temperature | NCEP[a] | SSM/I[b] | NCEP[a] | Satellites and numerical weather prediction models | | |
| Bulk algorithm | Chou (1993) | Fairall et al. (1996); Fairall et al. (2003) | Fairall et al. (2003) | | unknown | Beljaars (1994, 1995) |

[a]National Centres for Environmental Prediction.
[b]Special Sensor Microwave/Imager.
[c]Advanced Microwave Scanning Radiometer–Earth Observing System.

similar spatial distribution with an equatorward increase, but the zonal symmetry is broken over some regions. The largest LHF (above 160 $Wm^{-2}$) appears over the region to the south of the African continent through which the warm Agulhas Current flows. With the eastward extension of the current, large LHF is also found over the southern Indian Ocean. The higher SST of warm currents increases the sea–air specific humidity difference, leading to greater LHF. For the same reason, the regions through which the warm East Australian and Brazil currents flow also display large LHF, whereas smaller LHF values are found over the regions through which the cold Falkland Current flows. Small values also appear over the Southern Ocean near the Antarctic continent, where SST is low. Although the overall spatial patterns are quite similar among the data sets, differences exist over some regions. For example, relatively large differences occur in the region of the Brazil Current, which is consistent with the results of Wainer et al. (2003) who compared four observation-based products and the model results of the National Center for Atmospheric Research's Community Climate System Model. The maximum value over the Agulhas current region also shows disparity among the data sets, with the highest value given by NCEP-2 (210 W $m^{-2}$) and the lowest by GSSTF-2 (170 W $m^{-2}$). Rouault et al. (2003) compared NCEP-2 and ERA-40 to in situ estimates and found that NCEP-2 and ERA-40 underestimate LHF and SHF over waters of the Agulhas Current during the austral autumn as a result of the poor SST spatial resolution.

An inter-comparison of the annual mean SHF of the six products is shown in Fig. 2. The SHF values are 3–4 times smaller than LHF. Except for HOAPS-3, the other five data sets show maximum SHF values in the regions where the largest LHF values appear. The largest SST–air temperature difference can explain this. However, for the HOAPS-3, the largest values of SHF exist over the southern Indian Ocean. Except for the Falkland cold region, most of the small values of SHF appear in the regions between 45°S and 55°S, which is different from the regions where low LHF values occur.

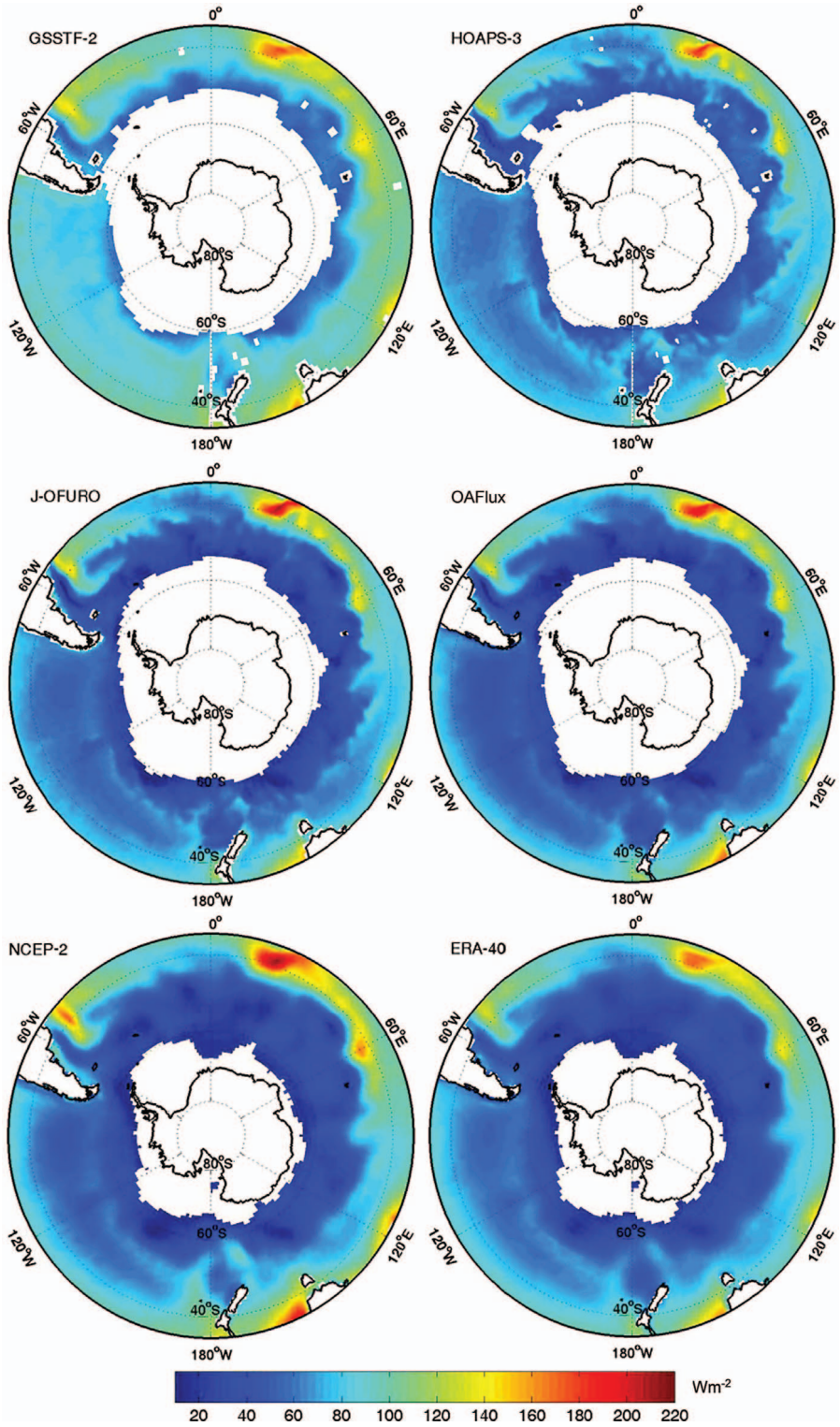


**Fig. 1** Annual mean latent heat flux over the Southern Ocean for the second version of the Goddard Satellite-Based Surface Turbulent Fluxes (GSSTF-2), the third version of the Hamburg Ocean Atmosphere Parameters and Fluxes from Satellite Data (HOAPS-3), Japanese Ocean Fluxes Data Sets with Use of Remote Sensing Observations (J-OFURO), Objectively Analyzed Air–Sea Fluxes for the Global Oceans (OAFlux), National Centers for Environmental Prediction Reanalysis 2 (NCEP-2) and the European Centre for Medium-Range Weather Forecasts 40 Year Re-analysis (ERA-40).



Citation: *Polar Research* 2011, *30*, 10167, DOI: 10.3402/polar.v30i0.10167

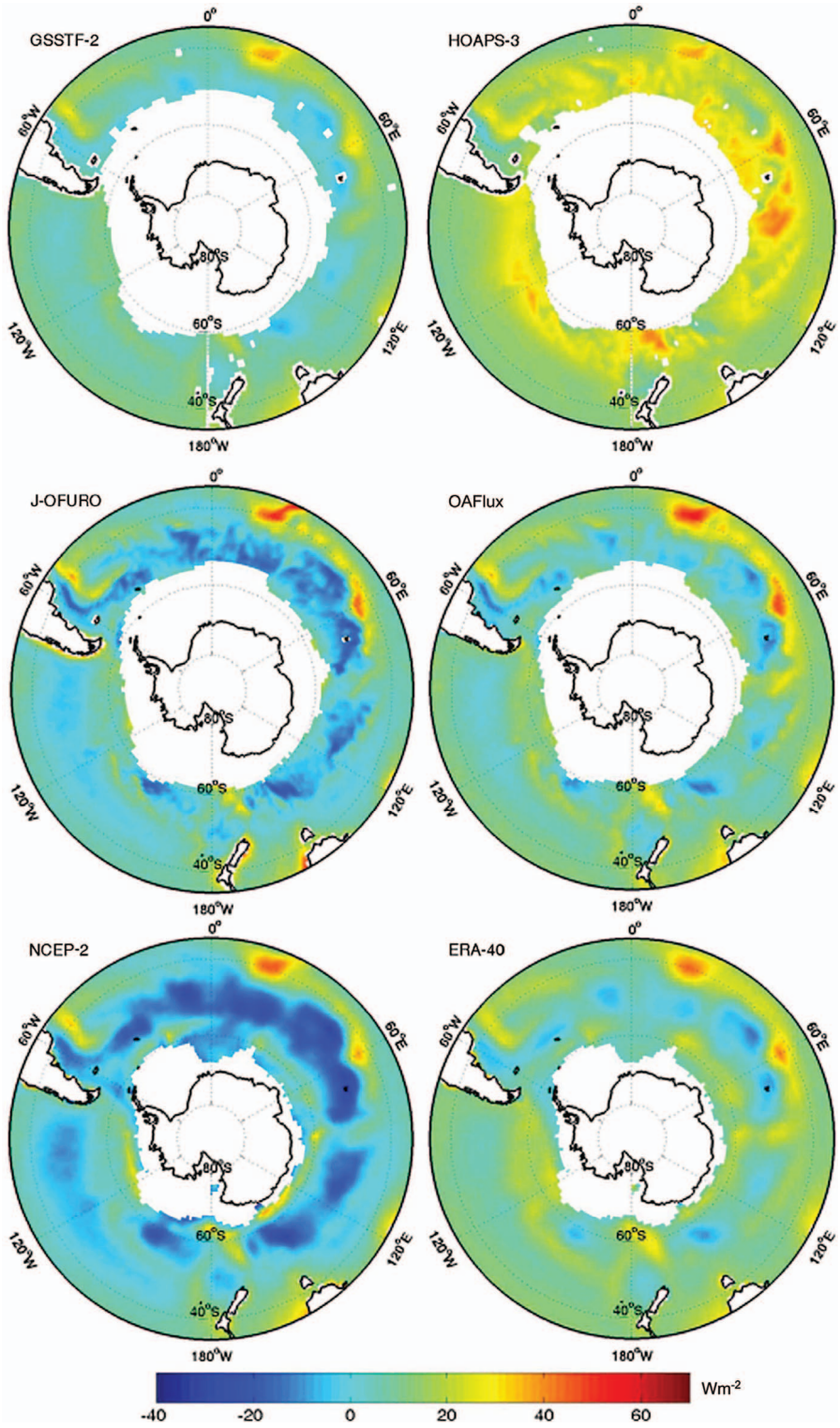


**Fig. 2** Annual mean sensible heat flux over the Southern Ocean for the second version of the Goddard Satellite-Based Surface Turbulent Fluxes (GSSTF-2), the third version of the Hamburg Ocean Atmosphere Parameters and Fluxes from Satellite Data (HOAPS-3), Japanese Ocean Fluxes Data Sets with Use of Remote Sensing Observations (J-OFURO), Objectively Analyzed Air–Sea Fluxes for the Global Oceans (OAFlux), National Centers for Environmental Prediction Reanalysis 2 (NCEP-2) and the European Centre for Medium-Range Weather Forecasts 40 Year Re-analysis (ERA-40).

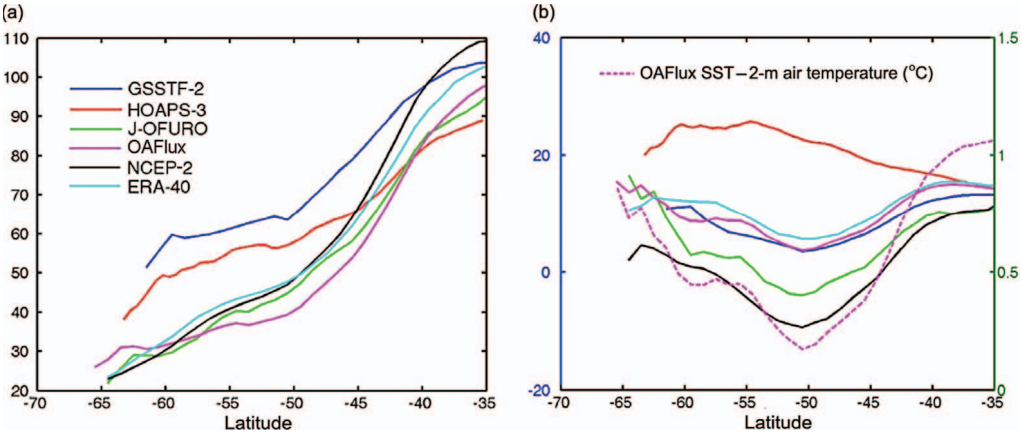


**Fig. 3** The meridional distribution of the zonal mean (a) latent heat flux and (b) sensible heat flux from the second version of the Goddard Satellite-Based Surface Turbulent Fluxes (GSSTF-2), the third version of the Hamburg Ocean Atmosphere Parameters and Fluxes from Satellite Data (HOAPS-3), Japanese Ocean Fluxes Data Sets with Use of Remote Sensing Observations (J-OFURO), Objectively Analyzed Air–Sea Fluxes for the Global Oceans (OAFlux), National Centers for Environmental Prediction Reanalysis 2 (NCEP-2) and the European Centre for Medium-Range Weather Forecasts 40 Year Re-analysis (ERA-40). Also shown in (b) is the meridional distribution of the sea surface temperature (SST) and 2-m air temperature difference from OAFlux.

To further study the meridional characteristics of LHF and SHF, we show the zonal-mean LHF and SHF as a function of latitude in Fig. 3. The LHF (Fig. 3a) over the Southern Ocean increases equatorward, but the rates of the increase or the meridional gradients differ among the six data sets. The GSSTF-2 and HOAPS-3 LHF share a similar pattern of variation with latitude, whereas the other four data sets are quite consistent in the rate of increase towards the equator. At most latitudes, the zonal mean GSSTF-2 LHF is larger than other five data sets. The pattern of the meridional variation of the zonal mean SHF (Fig. 3b) is significantly different from that of LHF. Unlike the LHF that displays a consistent equatorward increasing trend, five of the six data sets (with an exception of HOAPS-3) exhibit a minimum value near 50°S, with SHF values increasing both equatorward and poleward. This meridional variation pattern is consistent with the variation pattern of $T_S$–$T_A$ shown for OAFlux. The meridional distribution of the zonal mean SHF from the HOAPS-3 data is substantially different from the rest of the group, showing a weak maximum near 50°S and another near 60°S and a linear decreasing trend towards the equator from 50°S. Unfortunately, the temperature data from the HOAPS-3 data set are unavailable to explain the different behaviour. Among the five data sets that show similar meriodinal variation patterns, GSSTF-2, J-OFURO, OAFlux and ERA-40 are close in values that are consistently higher than J-OFURO and NCEP-2 at all latitudes. Another prominent feature in Fig. 3b is that the zonal mean SHF values in NCEP-2 are consistently lower than the other data sets and even become negative between about 57°S and 45°S, whereas the zonal mean SHF in the other data sets are always positive. The negative zonal mean SHF in NCEP-2 results from negative values of SHF as a response to negative sea–air temperature differences over the southern Indian and Atlantic oceans.

The seasonal cycle of LHF and SHF from the six data products were compared using all-grid average value (no area weighting) south of 35°S (Fig. 4). A maximum of LHF and SHF appear in the winter months, whereas a minimum occur in summer. The seasonal cycle is largely due to the seasonal variation in wind speed (Yu et al. 2008), with strong winds in winter and weak winds in summer. Throughout all seasons, the GSSTF-2 LHF and HOAPS-3 SHF values are consistently the largest among the six data sets, which is consistent with the zonal mean values. The seasonal variations of LHF and SHF in the HOAPS-3 data set are stronger than the other five data sets, especially for SHF.

## Inter-annual variation

The standard deviation for the annual mean LHF and SHF are shown in Figs. 5 and 6. Higher standard deviations indicate larger inter-annuall variability. For LHF, the spatial pattern of standard deviation is quite similar to the spatial distribution of the annual mean LHF. The range of the standard deviation is the largest (1.5–20.2 W $m^{-2}$) in J-OFURO and smallest (0.6–10.6 W $m^{-2}$) in ERA-40. There is little seasonal



Citation: *Polar Research* 2011, *30*, 10167, DOI: 10.3402/polar.v30i0.10167

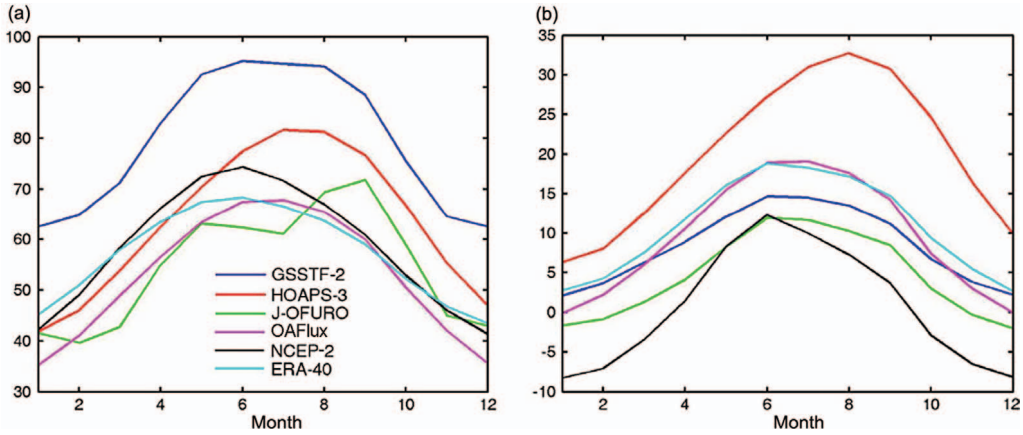


**Fig. 4** Seasonal cycle of values averaged over regions south of 35 °S for (a) latent heat flux and (b) sensible heat flux from the second version of the Goddard Satellite-Based Surface Turbulent Fluxes (GSSTF-2), the third version of the Hamburg Ocean Atmosphere Parameters and Fluxes from Satellite Data (HOAPS-3), Japanese Ocean Fluxes Data Sets with Use of Remote Sensing Observations (J-OFURO), Objectively Analyzed Air–Sea Fluxes for the Global Oceans (OAFlux), National Centers for Environmental Prediction Reanalysis 2 (NCEP-2) and the European Centre for Medium-Range Weather Forecasts 40 Year Re-analysis (ERA-40).

variation in the standard deviation (not shown). Unlike LHF, the spatial distribution of the standard deviation for annual mean SHF is different from the distribution of annual mean SHF values. For HOAPS-3, J-OFURO, OAFlux and ERA-40, the greatest inter-annual variation occurs over the south-east region of the Pacific Southern Ocean; for GSSTF-2 the maximum value appears over the ocean south of South Africa; for NCEP-2 the maximum value of 23.7 W $m^{-2}$ appears over the ocean to the north of Wilkes Land. Some seasonal variations are found in the standard deviation for SHF with the largest inter-annual variability in the winter season and the smallest in the summer.

In addition, the brevity of the time series (13 years) may degrade the number of independent samples. This is why we tested for variance difference of the area-averaged LHF and SHF for the six products. Only the variance differences between GSSTF-2 SHF and the other five products exceed the 95% confidence level. That indicates a consistent standard deviation of inter-annual variation of heat fluxes.

The Antarctic Oscillation (AAO) is the first mode of 700-mb geopotential height poleward of 20°S, which refers to a large-scale alternation of atmospheric mass between mid-latitude and high latitude (Thompson & Wallace 2000). Previous studies have indicated that AAO exerts its strong impact on LHF and SHF over the Southern Ocean (Sen Gupta & England 2006). To examine how the six data sets capture the relationship between AAO and LHF/SHF, we calculated the correlation coefficients between LHF and SHF and the AAO index obtained from the National Oceanic and Atmospheric Administration Climate Prediction Center (http://www.cpc.ncep.noaa.gov/products/precip/CWlink/daily_ao_index/aao/aao_index.html). Because the maximum LHF and SHF occur in austral winter (June, July and August; Fig. 4), the results are shown for the winter season only (Figs. 7, 8). The regions with positive correlation between LHF and AAO index (Fig. 7) include the central Pacific Southern Ocean and Indian Southern Ocean south of 45°S, whereas the Atlantic Southern Ocean and the ocean near New Zealand exhibit a negative correlation. The six products show a similar correlation pattern, but small differences exist over the East Antarctic coastal ocean and the Bellingshausen Sea. A similar spatial pattern of the correlation coefficients exists for SHF. Correlation coefficients for other seasons (not shown) display a more or less consistent spatial pattern over most of the Southern Ocean. The spatial patterns of the AAO–LHF/SHF correlation appear to be closely associated with the effect of AAO on SST, air temperature and humidity.

At Southern Hemispheric extratropical latitudes, the second and third modes of empirical orthogonal function (EOF) analysis of 700 hPa geopotential height depict wave-3 patterns in quadrature with each other and a well-defined wave train from the tropical western Pacific to Argentina, with large amplitudes in the Pacific–South American sector that are referred to as the PSA teleconnection patterns (Ghil & Mo 1991). Due to one-fourth phase difference of the two modes, the effects of the PSA1 on LHF and SHF are taken into account. Like the AAO index, the impact of the PSA1on LHF/SHF is compared for only the winter season (Figs. 9, 10). For

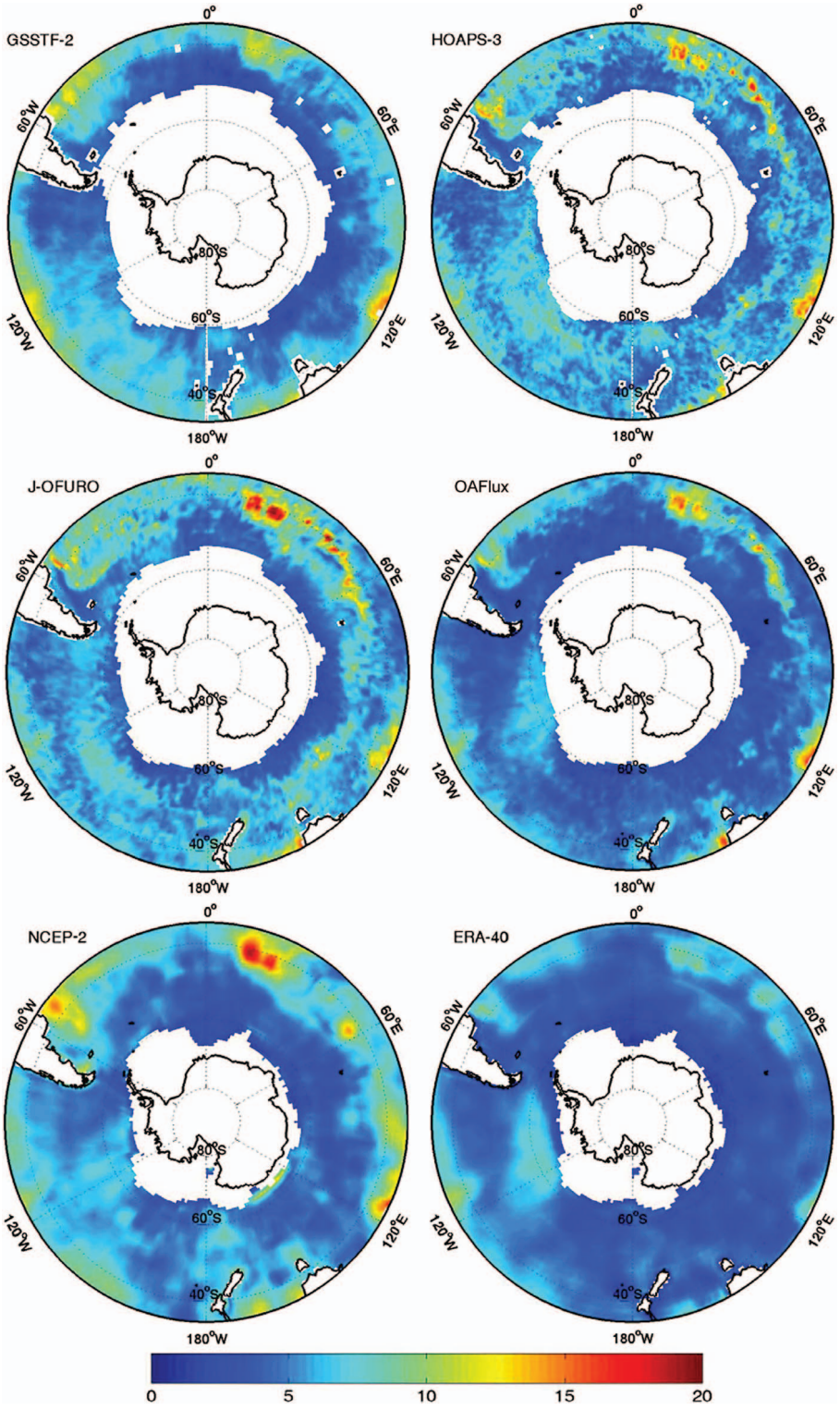


**Fig. 5** Standard deviation of annual mean latent heat flux over the Southern Ocean for the second version of the Goddard Satellite-Based Surface Turbulent Fluxes (GSSTF-2), the third version of the Hamburg Ocean Atmosphere Parameters and Fluxes from Satellite Data (HOAPS-3), Japanese Ocean Fluxes Data Sets with Use of Remote Sensing Observations (J-OFURO), Objectively Analyzed Air–Sea Fluxes for the Global Oceans (OAFlux), National Centers for Environmental Prediction Reanalysis 2 (NCEP-2) and the European Centre for Medium-Range Weather Forecasts 40 Year Re-analysis (ERA-40).



Citation: *Polar Research* 2011, *30*, 10167, DOI: 10.3402/polar.v30i0.10167

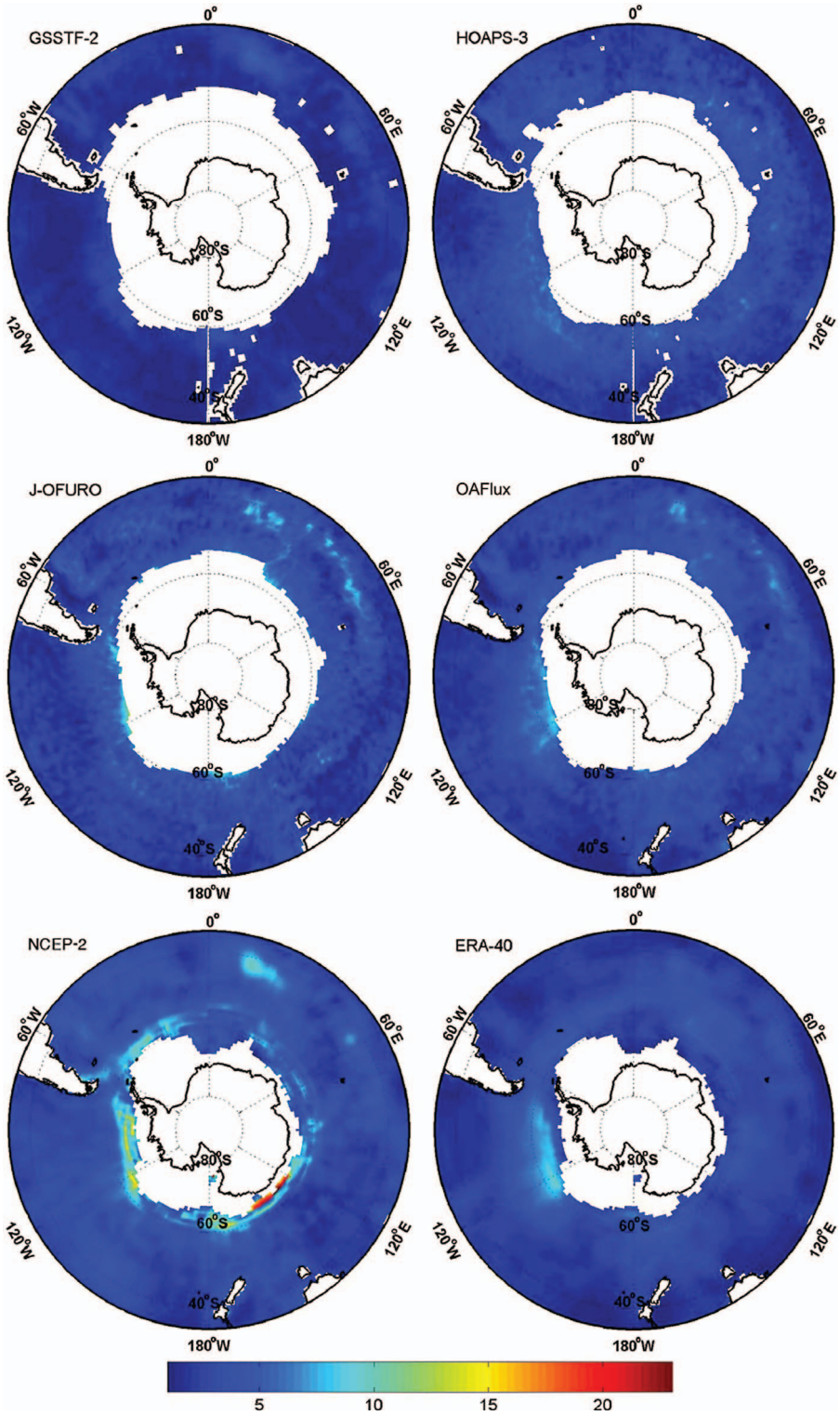


**Fig. 6** Standard deviation of annual mean sensible heat flux over the Southern Ocean for the second version of the Goddard Satellite-Based Surface Turbulent Fluxes (GSSTF-2), the third version of the Hamburg Ocean Atmosphere Parameters and Fluxes from Satellite Data (HOAPS-3), Japanese Ocean Fluxes Data Sets with Use of Remote Sensing Observations (J-OFURO), Objectively Analyzed Air–Sea Fluxes for the Global Oceans (OAFlux), National Centers for Environmental Prediction Reanalysis 2 (NCEP-2) and the European Centre for Medium-Range Weather Forecasts 40 Year Re-analysis (ERA-40).

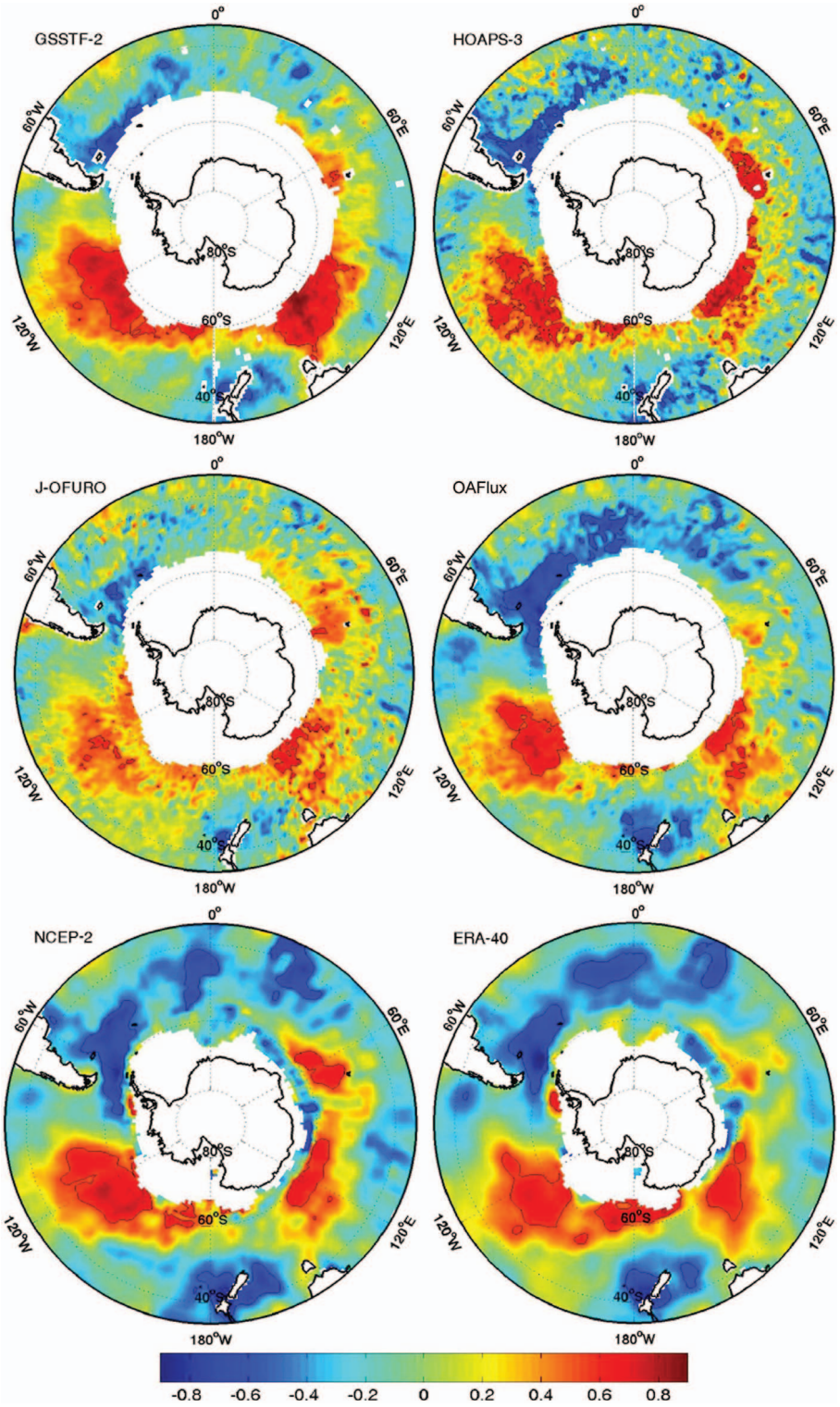


**Fig. 7** Winter season correlation coefficients between the Antarctic Oscillation index and latent heat flux for the second version of the Goddard Satellite-Based Surface Turbulent Fluxes (GSSTF-2), the third version of the Hamburg Ocean Atmosphere Parameters and Fluxes from Satellite Data (HOAPS-3), Japanese Ocean Fluxes Data Sets with Use of Remote Sensing Observations (J-OFURO), Objectively Analyzed Air–Sea Fluxes for the Global Oceans (OAFlux), National Centers for Environmental Prediction Reanalysis 2 (NCEP-2) and the European Centre for Medium-Range Weather Forecasts 40 Year Re-analysis (ERA-40). Thin black lines indicate regions with correlation coefficients above the 95% confidence level.



Citation: *Polar Research* 2011, *30*, 10167, DOI: 10.3402/polar.v30i0.10167

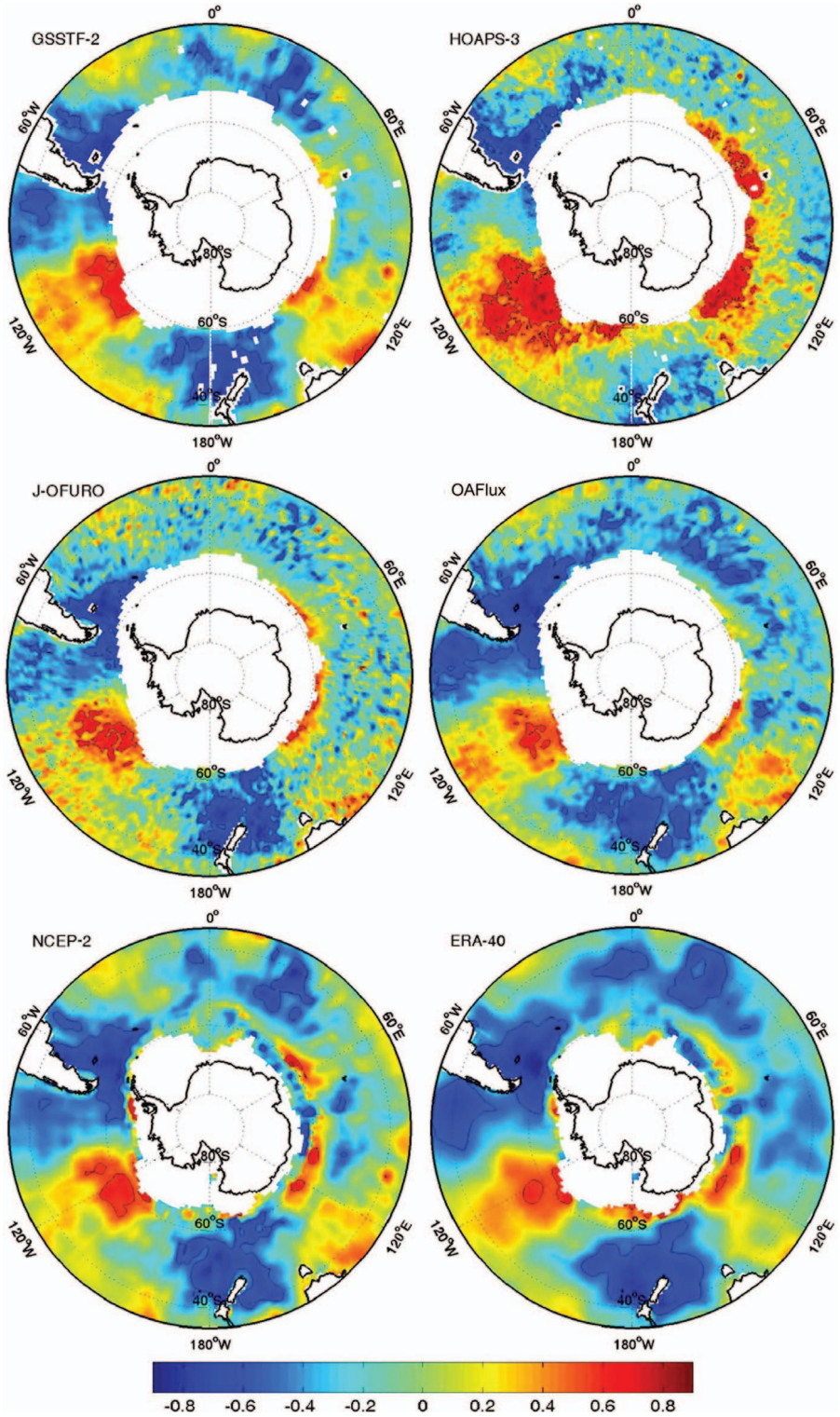


**Fig. 8** Winter season correlation coefficients between the Antarctic Oscillation index and sensible heat flux for the second version of the Goddard Satellite-Based Surface Turbulent Fluxes (GSSTF-2), the third version of the Hamburg Ocean Atmosphere Parameters and Fluxes from Satellite Data (HOAPS-3), Japanese Ocean Fluxes Data Sets with Use of Remote Sensing Observations (J-OFURO), Objectively Analyzed Air–Sea Fluxes for the Global Oceans (OAFlux), National Centers for Environmental Prediction Reanalysis 2 (NCEP-2) and the European Centre for Medium-Range Weather Forecasts 40 Year Re-analysis (ERA-40). Thin black lines indicate regions with correlation coefficients above the 95% confidence level.

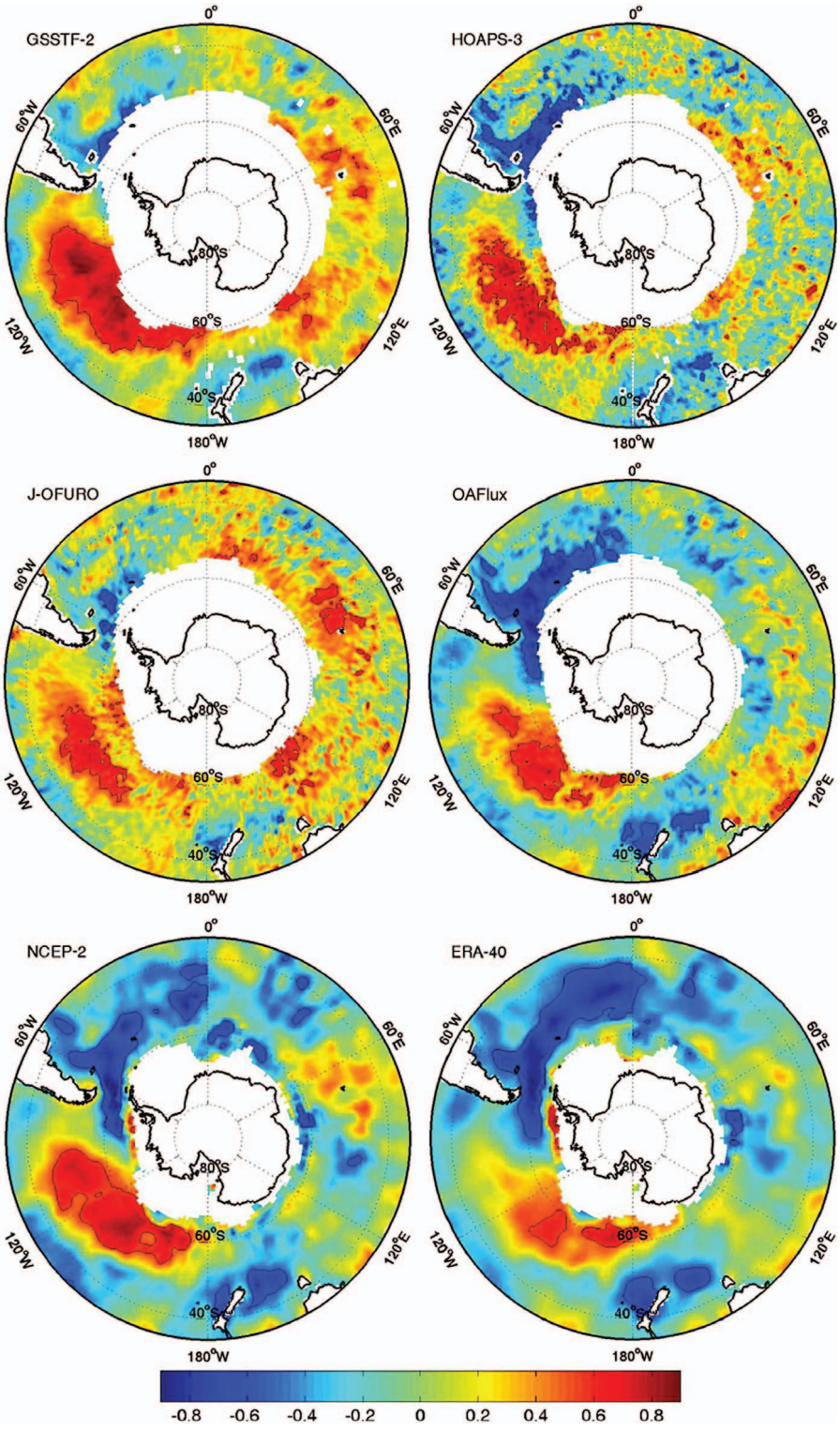


**Fig. 9** Winter season correlations of Pacific-South American index and latent heat flux for the second version of the Goddard Satellite-Based Surface Turbulent Fluxes (GSSTF-2), the third version of the Hamburg Ocean Atmosphere Parameters and Fluxes from Satellite Data (HOAPS-3), Japanese Ocean Fluxes Data Sets with Use of Remote Sensing Observations (J-OFURO), Objectively Analyzed Air–Sea Fluxes for the Global Oceans (OAFlux), National Centers for Environmental Prediction Reanalysis 2 (NCEP-2) and the European Centre for Medium-Range Weather Forecasts 40 Year Re-analysis (ERA-40). Thin black lines indicate regions with correlation coefficients above the 95% confidence level.



Citation: *Polar Research* 2011, *30*, 10167, DOI: 10.3402/polar.v30i0.10167

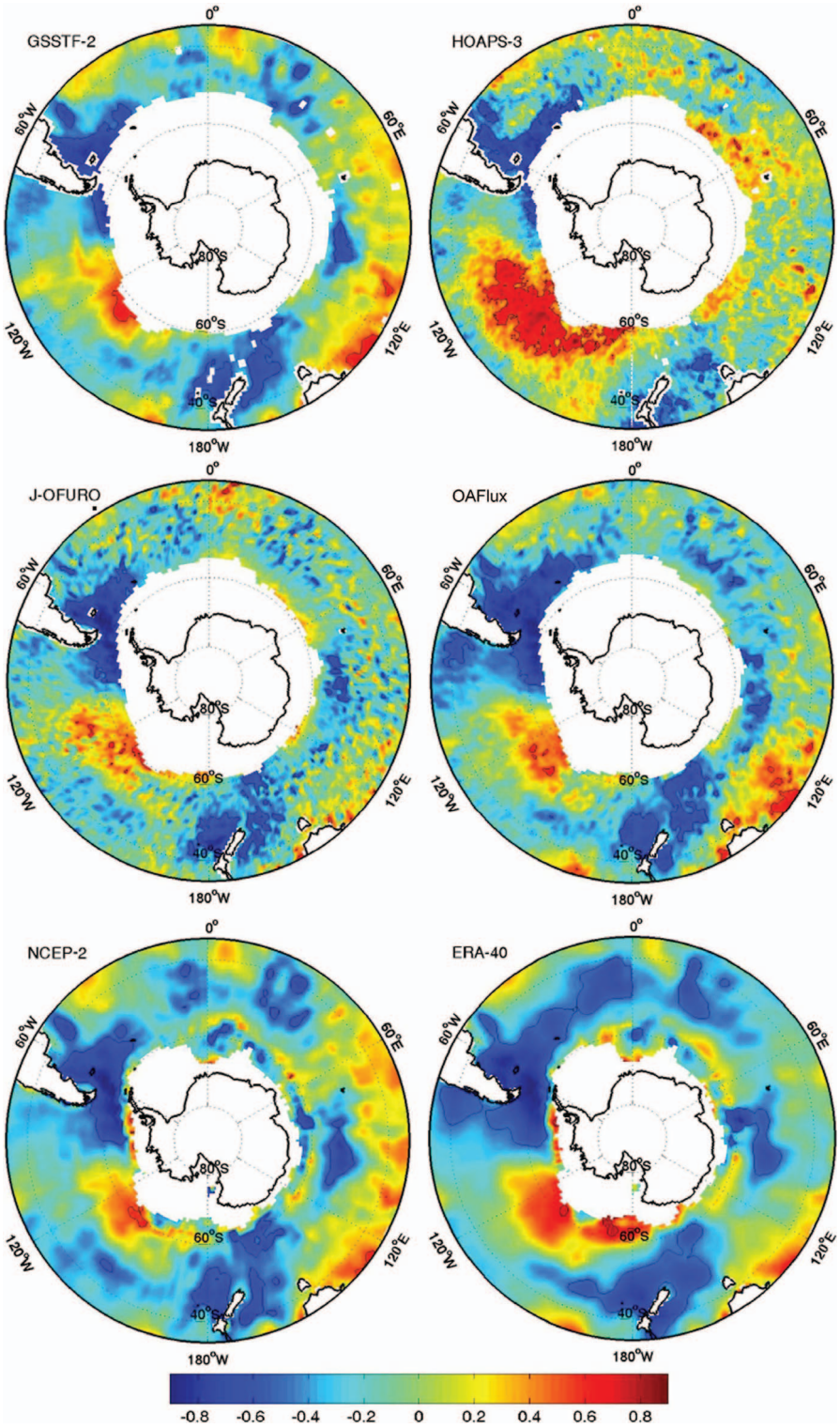


**Fig. 10** Winter season correlations of Pacific-South American index and sensible heat flux for the second version of the Goddard Satellite-Based Surface Turbulent Fluxes (GSSTF-2), the third version of the Hamburg Ocean Atmosphere Parameters and Fluxes from Satellite Data (HOAPS-3), Japanese Ocean Fluxes Data Sets with Use of Remote Sensing Observations (J-OFURO), Objectively Analyzed Air–Sea Fluxes for the Global Oceans (OAFlux), National Centers for Environmental Prediction Reanalysis 2 (NCEP-2) and the European Centre for Medium-Range Weather Forecasts 40 Year Re-analysis (ERA-40). Thin black lines indicate regions with correlation coefficients above the 95% confidence level.

LHF, the most significant positive correlation regions are distributed over the Pacific Southern Ocean, whereas the significant negative correlation occurs over the Atlantic Southern Ocean and the ocean near New Zealand. The largest difference of PSA1 correlation among the six products exists in the Indian Southern Ocean, where the PSA1 index does not have a strong impact on meteorological variables. The most significant positive correlation between the SHF and PSA1 occurs over the Pacific Southern Ocean and in the HOAPS-3 data set, the correlations in other data sets are less pronounced. However, the ocean near New Zealand, the south-east Pacific Ocean and the Atlantic Southern Ocean show the strongest negative correlation in the ERA-40 data set. Overall, the correlation between the heat fluxes and PSA index shows a similar spatial pattern among the six data sets. The regions of positive (negative) correlation respond to negative (positive) pressure anomaly. The reason may be that the cyclonic circulation contributes to increasing the humidity and temperature differences between the ocean surfaces and the atmosphere above.

In addition, we also considered the effect of three indices on the bulk variables. For the AAO index, ocean–2-m air temperature and specific humidity difference show a zonal three-wave structure over the Southern Ocean, whose spatial patterns are in agreement with those of SHF and LHF; for 10-m wind speed, a significant increase occurs south of 50°S from 0° to 90°W with opposite correlation coefficient north of 50°S (not shown). The spatial structures of correlation between ocean–2-m air temperature and specific humidity and the PSA1 and PSA2 indices are similar to those of SHF and LHF. For wind speed, spatial patterns of the PSA1 and PSA2 indices show two- and three-wave structures.

Leading EOF patterns can be a good tool to examine the dominant mode of variability in each flux product for a short time series. Using EOF analysis, we find that the first mode pattern of LHF shows a consistent zonal three-wave structure except for J-OFURO, where the structure is zonally symmetrical, but the pattern of SHF shows a similar three-wave structure for the six products being compared (not shown).

## Decadal trend

The linear trends of LHF and SHF in 13 years for the six data sets are shown in Figs. 11 and 12. The positive trends in LHF are widely distributed over the Southern Ocean, with more significant trends over the oceans where the annual mean values are large. The negative trends occur at the Bellingshausen Sea, the Amundsen Sea and the Southern Indian Ocean. A strong decreasing trend of more than 30 W $m^{-2}$ in 13 years appears over the oceans to the north of Wilkes Land in the NCEP-2 data set, and the weakest negative trend of LHF (only about 5 W $m^{-2}$ in 13 years) is associated with the GSSTF-2 data set. The positive trends in ERA-40 appear to be much weaker compared to those in other five data sets.

Compared to LHF, the trend difference for SHF among the data sets is larger. NCEP-2 shows the largest decreasing trend of SHF: more than 60 W $m^{-2}$ in 13 years over the ocean to the north of Wilkes Land, where the trend in LHF is also negative. GSSTF-2 exhibits the weakest decreasing trend of SHF: less than 5 W $m^{-2}$ in 13 years. However, the behaviour of the positive trend among the data sets is somewhat different. The largest positive trend of over 30 W $m^{-2}$ in 13 years appears over the ocean south of South Africa in NCEP-2, where other data sets also show a significant positive trend, with ERA-40 having the smallest value of about 10 W $m^{-2}$ in 13 years.

The trend differences of LHF and SHF among the six data sets may be attributed to a number of factors. The difference in wind speed and sea–air specific humidity will be examined in the following section. The temperature differences will not be discussed here because several data sets do not contain either SST or air temperature data.

## Influences of bulk meteorological parameters

The differences for LHF and SHF may be caused by two primary sources: one is the differences in the bulk variables and the other is the differences in the algorithms themselves (Brunke et al. 2002). In this article, we will focus on the bulk variables, specifically wind speed and temperature and humidity differences. Wind speeds and humidity differences are calculated for all six data sets. The sources of air temperature and SST for GSSTF-2 and J-OFURO are NCEP-2; the air temperature and SST for HOAPS-3 cannot be obtained from its website. Therefore, the effect of $T_S$–$T_A$ on sensible heat flux is limited to NCEP-2, ERA-40 and OAFlux.

The annual mean of wind speed exhibits a similar spatial pattern among the six data sets, with larger values over oceans between 40°S and 60°S (not shown). The annual mean of the sea and air specific humidity difference from the six data sets also shows a consistent spatial pattern (not shown). The annual means of the sea and air temperature from NCEP-2, ERA-40 and OAFlux are similar (not shown). The spatial patterns of annual mean difference between specific humidity over the ocean surface and the air ($Q_S$–$Q_A$) and sea–air temperature difference ($T_S$–$T_A$) are in line with those of LHF and



Citation: *Polar Research* 2011, *30*, 10167, DOI: 10.3402/polar.v30i0.10167

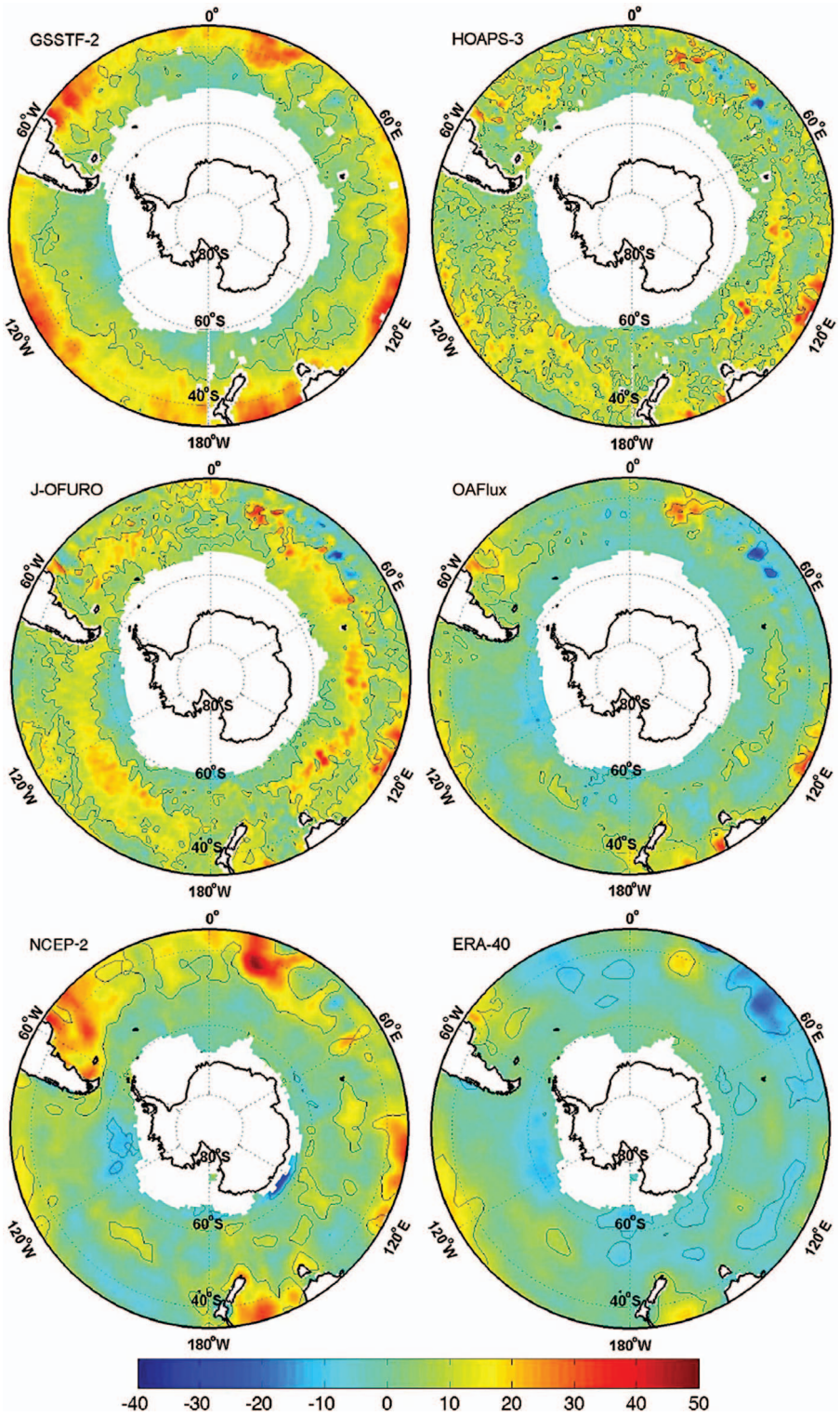


**Fig. 11** The linear trends of annual mean latent heat flux over the Southern Ocean for the second version of the Goddard Satellite-Based Surface Turbulent Fluxes (GSSTF-2), the third version of the Hamburg Ocean Atmosphere Parameters and Fluxes from Satellite Data (HOAPS-3), Japanese Ocean Fluxes Data Sets with Use of Remote Sensing Observations (J-OFURO), Objectively Analyzed Air–Sea Fluxes for the Global Oceans (OAFlux), National Centers for Environmental Prediction Reanalysis 2 (NCEP-2) and the European Centre for Medium-Range Weather Forecasts 40 Year Re-analysis (ERA-40). Thin black lines indicate regions with correlation coefficients above the 90% confidence level.

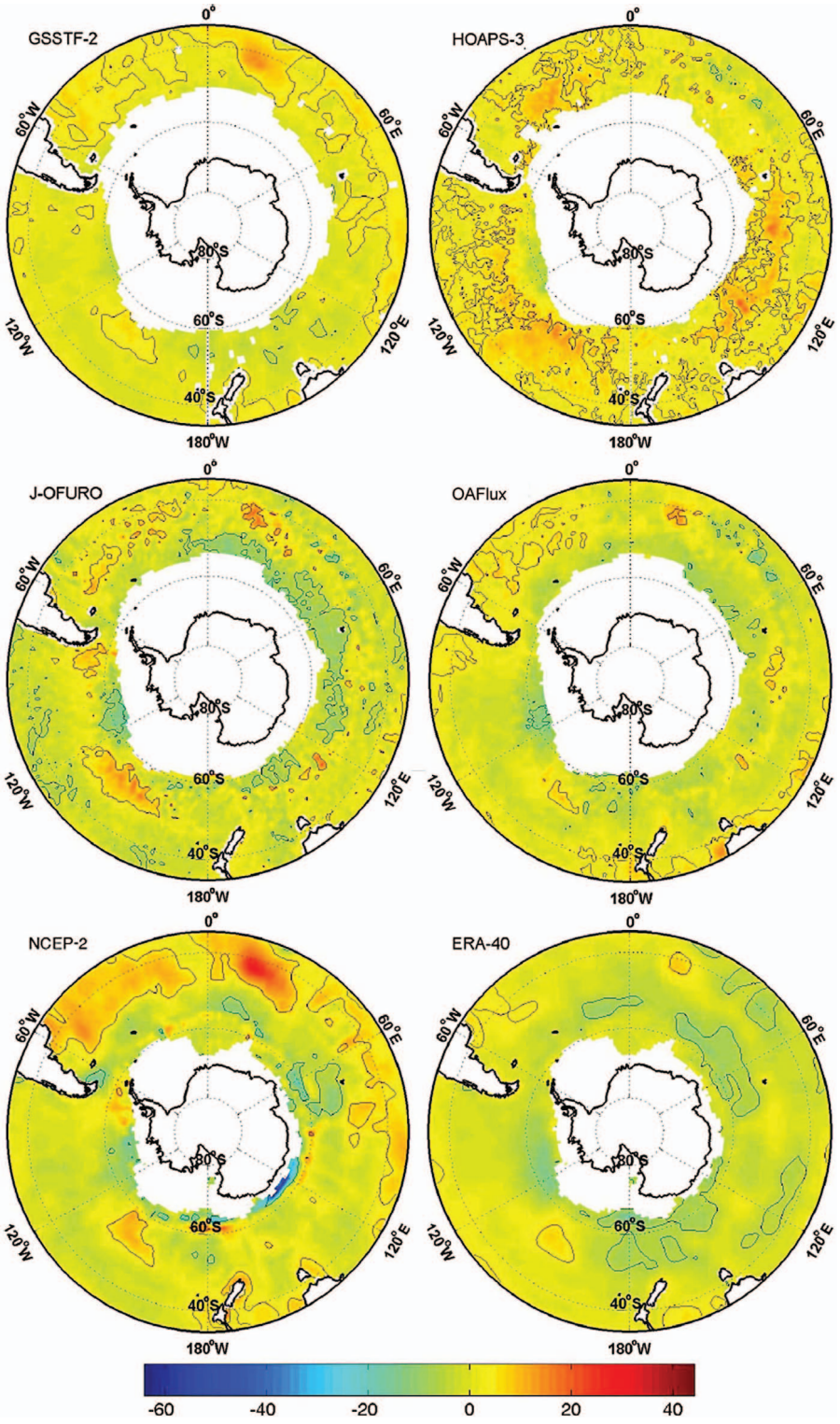


**Fig. 12** The linear trends of annual mean sensible heat flux over the Southern Ocean for the second version of the Goddard Satellite-Based Surface Turbulent Fluxes (GSSTF-2), the third version of the Hamburg Ocean Atmosphere Parameters and Fluxes from Satellite Data (HOAPS-3), Japanese Ocean Fluxes Data Sets with Use of Remote Sensing Observations (J-OFURO), Objectively Analyzed Air–Sea Fluxes for the Global Oceans (OAFlux), National Centers for Environmental Prediction Reanalysis 2 (NCEP-2) and the European Centre for Medium-Range Weather Forecasts 40 Year Re-analysis (ERA-40). Thin black lines indicate regions with correlation coefficients above the 90% confidence level.



Citation: *Polar Research* 2011, *30*, 10167, DOI: 10.3402/polar.v30i0.10167

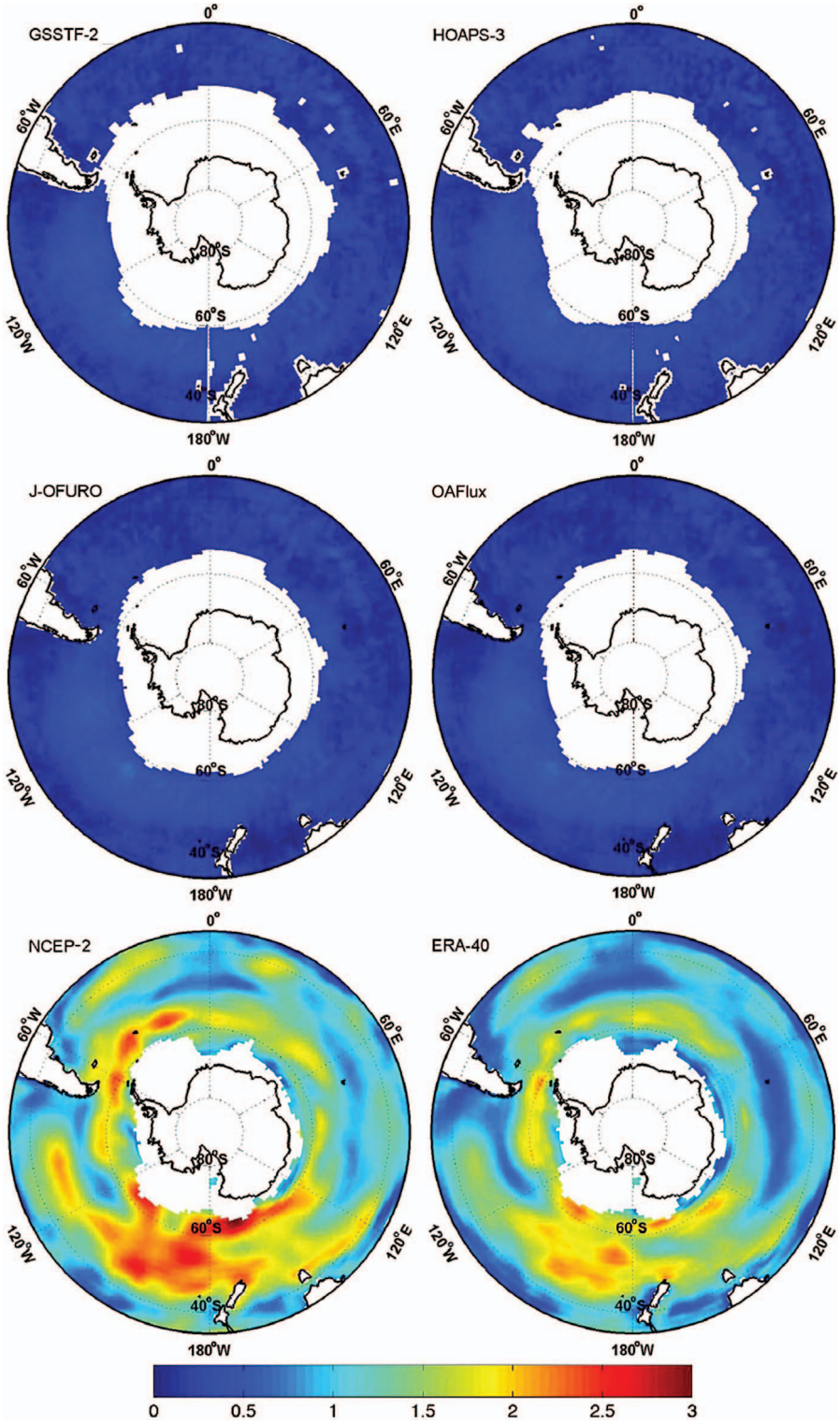


**Fig. 13** Standard deviation of annual mean wind speed over the Southern Ocean for the second version of the Goddard Satellite-Based Surface Turbulent Fluxes (GSSTF-2), the third version of the Hamburg Ocean Atmosphere Parameters and Fluxes from Satellite Data (HOAPS-3), Japanese Ocean Fluxes Data Sets with Use of Remote Sensing Observations (J-OFURO), Objectively Analyzed Air–Sea Fluxes for the Global Oceans (OAFlux), National Centers for Environmental Prediction Reanalysis 2 (NCEP-2) and the European Centre for Medium-Range Weather Forecasts 40 Year Re-analysis (ERA-40).

SHF, respectively. Here, we mainly focus on the standard deviation and trend of wind speed, $Q_S$–$Q_A$ and $T_S$–$T_A$.

Figure 13 shows that a consistent spatial pattern of standard deviation of wind speed occurs among three satellite-derived products and OAFlux with larger variation over the southern Pacific Ocean. The range of variation of the standard deviation is also similar, from 0.1 to 0.7 $ms^{-1}$. The two re-analysis data sets share a similar spatial pattern and their ranges of variation exceed those in the other four data sets. Feng & Li (2006) also found large difference in the standard deviation of wind speed between GSSTF-2 and NCEP-2 at southern high latitudes. The spatial patterns of standard deviation of wind speed do not appear to correspond well with the pattern of LHF and SHF, suggesting that other factors may play a more important role in standard deviations of LHF and SHF. Like the annual mean, the standard deviation of $Q_S$–$Q_A$ among the six products also displays a similar pattern (Fig. 14) that coincides with the spatial pattern of LHF, indicating that the humidity difference between the ocean and air plays a significant role in determining the inter-annual variation of LHF over the Southern Ocean.

In the case of the linear trend of wind speed (Fig. 15), differences among the six data sets are similar to those of standard deviation. In other words, the trends are larger in the two re-analysis data sets compared to those in the other four data sets. Despite the differences in the magnitudes, all six products display a similar spatial pattern with larger trend appearing over the southern Indian Ocean and oceans between 180° and 120°E south of 50°S. The largest difference between the two re-analysis data sets and the other four data sets occurs over the south-western Atlantic Ocean, the south-western Pacific Ocean and the ocean south of Australia. The spatial patterns of the wind speed trend for all six products do not appear to correspond with the spatial pattern of LHF and SHF. In contrast, the spatial distribution of the $Q_S$–$Q_A$ trend (Fig. 16) appears to coincide with that of LHF, although differences exist in the range of trends among the products. This indicates that the LHF trends are closely related to that of $Q_S$–$Q_A$. The results here appear to differ from the results of Kubota et al. (2003), which revealed a bigger contribution from wind speed to the differences between two satellite-derived flux products. However, the work of (Feng & Li 2006: figures 5, 6) appears to support our results, which showed that the differences of LHF over the Southern Ocean between GSSTF-2 and the re-analysis data sets may be caused by the difference in $Q_S$–$Q_A$. Liu and Curry (2006) also found some discrepancies on the spatial/temporal variations of the LHF caused by the air specific humidity over the tropics and subtropics.

The patterns of standard deviations and trends of $T_S$–$T_A$ for OAFlux, NCEP-2 and ERA-40 are shown in Fig. 17. The spatial patterns of standard deviation for three products are similar to those of sensible heat flux. The large inter-annual variation occurs over the coastal ocean near the Antarctica and over the southern Indian Ocean. The patterns of the trends in $T_S$–$T_A$ for the three products are also consistent with those of sensible heat flux. A significantly positive trend occurs mainly over the south-western Atlantic Ocean and southern Indian Ocean, and a negative trend exists over the coastal ocean near the Antarctic continent. In terms of value, the contribution of $T_S$–$T_A$ in ERA-40 to the trend in SHF is less than that of other two products.

## Conclusions

This study compares LHF and SHF among six gridded data sets, namely, GSSTF-2, HOAPS-3, J-OFURO, OAFlux, NCEP-2 and ERA-40, over the Southern Ocean for the period of 1988 through 2000, when all six data sets overlap. The large-scale patterns of the 13-year mean fields for LHF, SHF and wind speed are similar among the data sets, but the values can differ substantially. The meridional characteristics of the zonal mean LHF are in good agreement among the six data sets, showing a continuous equatorward increase. The meridional distribution of zonal mean SHF is similar among five of the six data sets (HOAPS-3 is the exception), exhibiting a minimum value near 50°S, increasing both pole- and equatorward, which is consistent with the sea–air temperature difference.

Larger values of LHF and SHF are found during the austral winter, consistent with the seasonal cycle of wind speed over the region. Among the six data sets, the LHF in GSSTF-2 and SHF in HOAPS-3 appear to be the largest for all months.

The standard deviations of annual mean LHF for all six products show a similar spatial pattern that is similar to the annual mean LHF, despite some differences in values. In contrast, the standard deviations of annual mean SHF exhibit different patterns among the six products. The seasonality of LHF standard deviation is weaker than that of SHF. There appears to be a closer link between OAFlux and the two re-analysis data sets, while the three satellite-derived products are more closely related to each other.

The correlation between the wintertime AAO and LHF shows a similar spatial pattern among the data sets, with positive correlation over the central southern Pacific



Citation: *Polar Research* 2011, *30*, 10167, DOI: 10.3402/polar.v30i0.10167

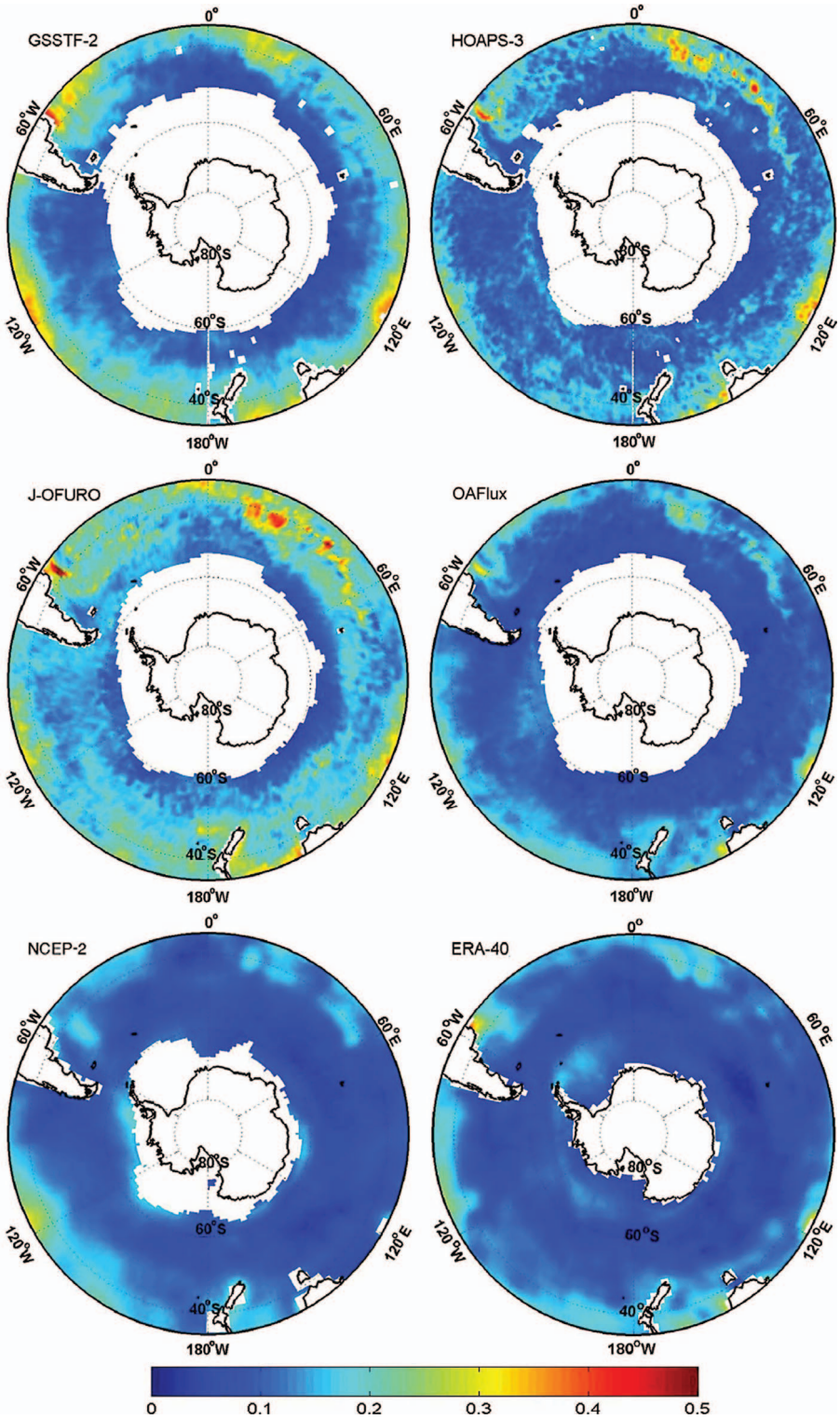


**Fig. 14** The standard deviations of the annual mean sea-air specific humidity difference over the Southern Ocean for the second version of the Goddard Satellite-Based Surface Turbulent Fluxes (GSSTF-2), the third version of the Hamburg Ocean Atmosphere Parameters and Fluxes from Satellite Data (HOAPS-3), Japanese Ocean Fluxes Data Sets with Use of Remote Sensing Observations (J-OFURO), Objectively Analyzed Air–Sea Fluxes for the Global Oceans (OAFlux), National Centers for Environmental Prediction Reanalysis 2 (NCEP-2) and the European Centre for Medium-Range Weather Forecasts 40 Year Re-analysis (ERA-40).

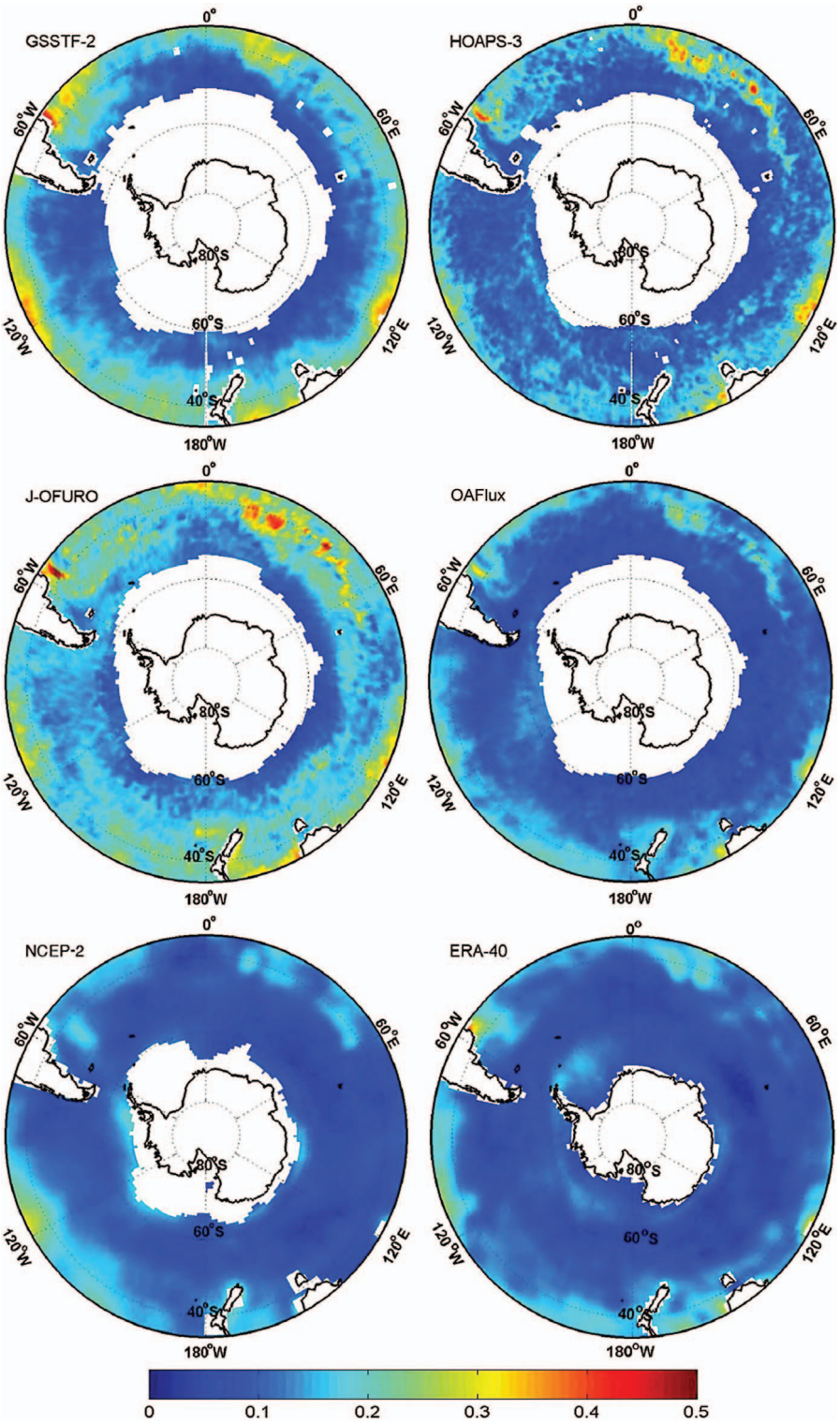


**Fig. 15** The linear trends of the annual mean wind speed over the Southern Ocean for the second version of the Goddard Satellite-Based Surface Turbulent Fluxes (GSSTF-2), the third version of the Hamburg Ocean Atmosphere Parameters and Fluxes from Satellite Data (HOAPS-3), Japanese Ocean Fluxes Data Sets with Use of Remote Sensing Observations (J-OFURO), Objectively Analyzed Air–Sea Fluxes for the Global Oceans (OAFlux), National Centers for Environmental Prediction Reanalysis 2 (NCEP-2) and the European Centre for Medium-Range Weather Forecasts 40 Year Re-analysis (ERA-40).



Citation: *Polar Research* 2011, *30*, 10167, DOI: 10.3402/polar.v30i0.10167

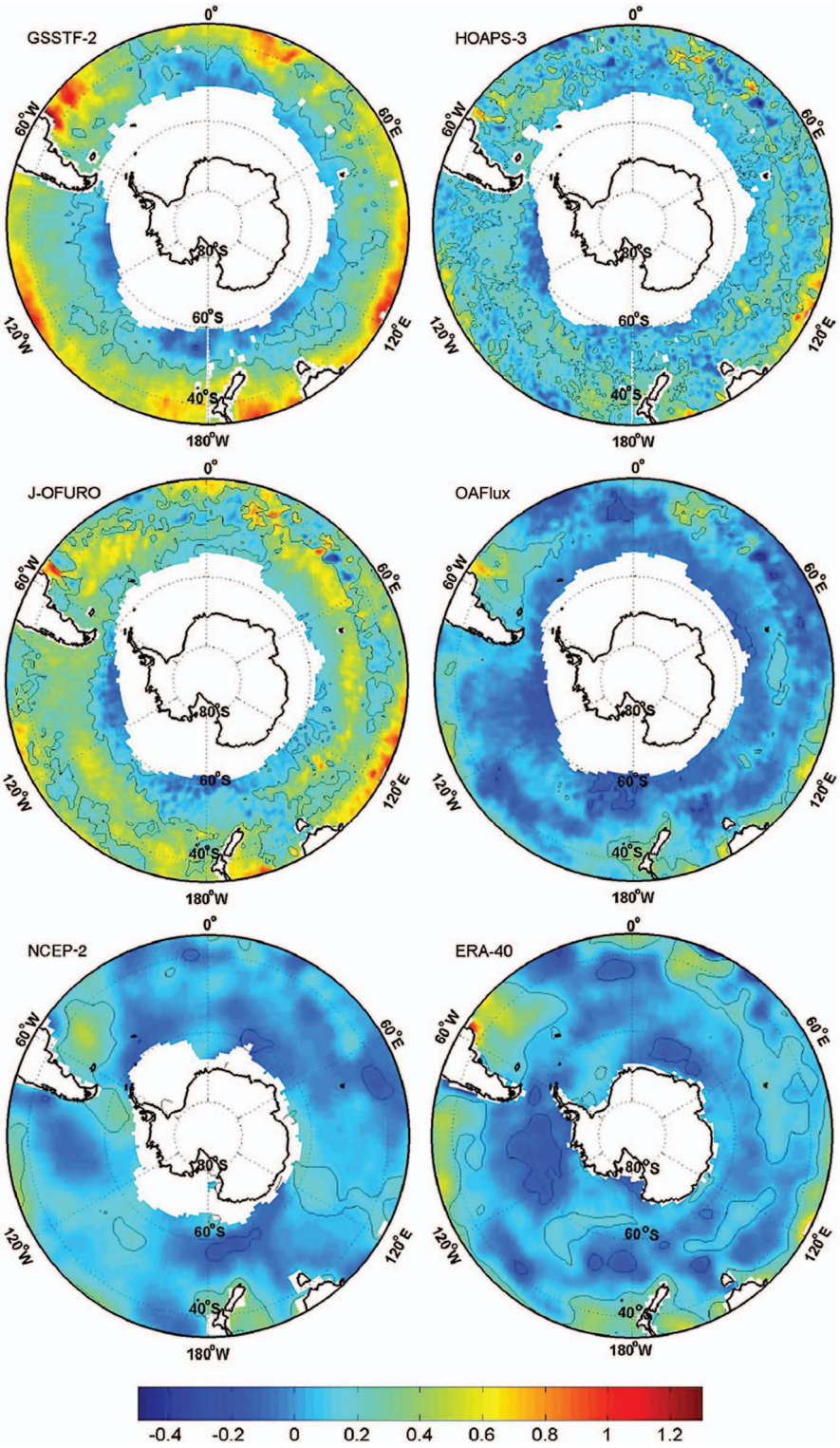


**Fig. 16** The linear trends of annual mean sea-air specific humidity difference over the Southern Ocean for the second version of the Goddard Satellite-Based Surface Turbulent Fluxes (GSSTF-2), the third version of the Hamburg Ocean Atmosphere Parameters and Fluxes from Satellite Data (HOAPS-3), Japanese Ocean Fluxes Data Sets with Use of Remote Sensing Observations (J-OFURO), Objectively Analyzed Air–Sea Fluxes for the Global Oceans (OAFlux), National Centers for Environmental Prediction Reanalysis 2 (NCEP-2) and the European Centre for Medium-Range Weather Forecasts 40 Year Re-analysis (ERA-40). Thin black lines indicate regions with correlation coefficients above the 90% confidence level.

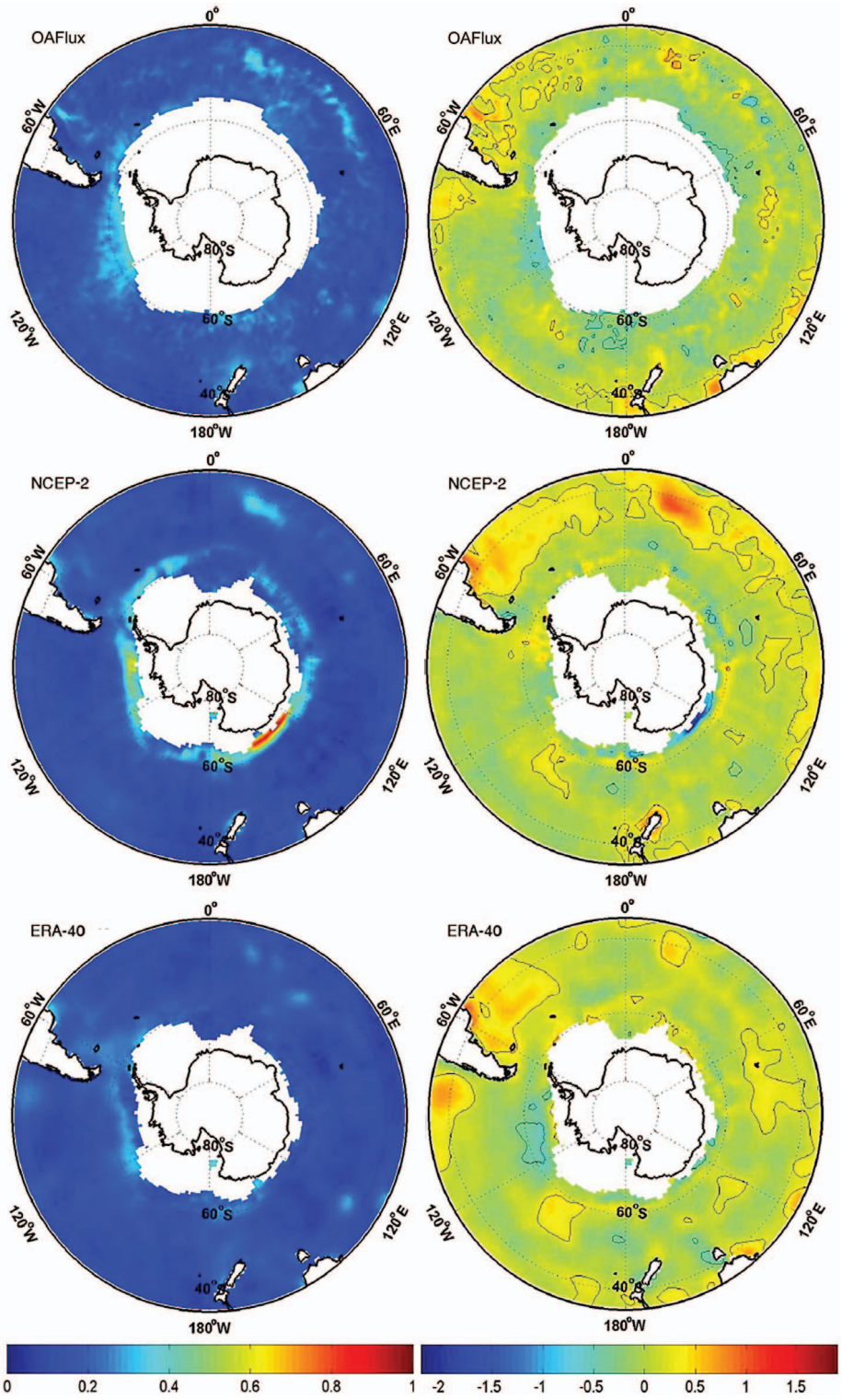


**Fig. 17** Standard deviation (left column) and trend (right column) of sea-air temperature difference for Objectively Analyzed Air–Sea Fluxes for the Global Oceans (OAFlux), National Centers for Environmental Prediction Reanalysis 2 (NCEP-2) and the European Centre for Medium-Range Weather Forecasts 40 Year Re-analysis (ERA-40). Thin black lines indicate regions with correlation coefficients above the 90% confidence level.



Citation: *Polar Research* 2011, *30*, 10167, DOI: 10.3402/polar.v30i0.10167

Ocean, the ocean south of Australia and the southern Indian Ocean and negative correlation over the southern Atlantic Ocean and the ocean near New Zealand. A significant correlation between the wintertime PSA and LHF is found over the southern Pacific Ocean in all six products. A common region with high PSA–SHF correlation is over the south-western Atlantic Ocean. Results for other seasons are similar with those for the austral winter.

The linear trend analysis of the annual mean fluxes shows significant differences in both the spatial pattern and the values. The differences in spatial distribution do not appear to be linked to the bulk parameter of mean wind speed, but related to the temperature and humidity differences between the ocean surface and the atmosphere. The trend and standard deviation of wind speed in the re-analysis data sets are found to be larger than those in the satellite-based data sets.

## Acknowledgements

This study was supported by the key project of the National Natural Science Foundation of China (grant number: 40930848 and 41106164), the National High-Tech Research and Development Program of China (grant number: 2008AA09Z117) and the Ministry of Science and Technology of China (grant number: 2006BAB18B03 and 2006BAB18B05). The GSSTF-2 LHF were obtained from the GSSTF-2 website (http://apdrc.soest.hawaii.edu/datadoc/gsstf_mon.php). The HOAPS-3 heat fluxes were obtained from the HOAPS website (http://www.hoaps.zmaw.de/). The J-OFURO heat fluxes were obtained from the J-OFURO website (http://dtsv.scc.u-tokai.ac.jp/j-ofuro/). The OAFlux heat fluxes were obtained from the OAFlux website (http://oaflux.whoi.edu/). The NCEP-2 data were obtained from the Climate Diagnostics Center (http://www.esrl.noaa.gov/psd/). The ECMWF re-analysis data were obtained from the website http://data-portal.ecmwf.int/data/d/era40_moda/.

## References

Andersson A., Bakan S., Fennig K., Grassl H., Klepp C.-P. & Schulz J. 2007. *Hamburg Ocean Atmosphere Parameters and Fluxes from Satellite Data—HOAPS—monthly mean*. Hamburg: World Data Center for Climate. Doi: 10.1594/WDCC/HOAPS3_MONTHLY.

Beljaars A.C.M. 1994. The parameterization of surface fluxes in large scale models under free convection. *Quarterly Journal of the Royal Meteorological Society 121*, 255–270.

Beljaars A.C.M. 1995. The impact of some aspects of the boundary layer scheme in the ECMWF model. In: *Seminar proceedings on parameterization of sub-grid scale physical processes*. Pp. 125–161. Reading, MA: European Centre for Medium-Range Weather Forecasts.

Beljaars A.C.M. 1997. Air–sea interaction in the ECMWF model. In: *Seminar proceedings on atmosphere–surface interaction*. Pp. 33–52. Reading, MA: European Centre for Medium-Range Weather Forecasts.

Bentamy A., Katsaros K.B., Mestas-Nunez A.M., Drennan W.M., Forde E.B. & Roquet H. 2003. Satellite estimates of wind speed and latent heat flux over the global oceans. *Journal of Climate 16*, 637–656.

Bourras D. 2006. Comparison of five satellite-derived latent heat flux products to moored buoy data. *Journal of Climate 19*, 6292–6313.

Brunke M.A., Fairall C.W., Zeng X., Eymard L. & Curry J.A. 2003. Which bulk aerodynamic algorithms are least problematic in computing ocean surface turbulent fluxes? *Journal of Climate 16*, 619–635.

Brunke M.A., Zeng X. & Anderson S. 2002. Uncertainties in sea surface turbulent flux algorithms and data sets. *Journal of Geophysical Research—Oceans 107*, 3141, doi: 10.1029/2001JC000992.

Chou S.-H. 1993. A comparison of airborne eddy-correlation and bulk aerodynamic methods for ocean–air turbulent fluxes during cold-air outbreaks. *Boundary-Layer Meteorology 64*, 75–100.

Chou S.-H., Chou M.-D., Chan P.-K., Lin P.-H. & Wang K.-H. 2004. Tropical warm pool surface heat budgets and temperature: contrasts between 1997–98 El Niño and 1998–99 La Niña. *Journal of Climate 17*, 1845–1858.

Chou S.-H., Nelkin E., Ardizzone J. & Atlas R.M. 2004. A comparison of latent heat fluxes over global oceans for four flux products. *Journal of Climate 17*, 3974–3989.

Chou S.-H., Nelkin E., Ardizzone J., Atlas R.M. & Shie C.L. 2003. Surface turbulent heat and momentum fluxes over global oceans based on the Goddard satellite retrievals, version 2 (GSSTF2). *Journal of Climate 16*, 3256–3273.

Chou S.-H., Shie C.-L., Atlas R.M. & Ardizzone J. 1997. Air–sea fluxes retrieved from special sensor microwave imager data. *Journal of Geophysical Research—Oceans 102*, 12705–12726.

Chou S.-H., Zhao W. & Chou M.-D. 2000. Surface heat budgets and sea surface temperature in the Pacific warm pool during TOGA COARE. *Journal of Climate 13*, 634–649.

Curry J.A., Bentamy A., Bourassa M.A., Bourras D., Bradley E.F., Brunke M., Castro S., Chou S.H., Clayson C.A., Emery W.J., Eymard L., Cairall C.W., Kubota M., Lin B., Perrie W., Reeder R.A., Renfrew I.A., Rossow W.B., Schulz J., Smith S.R., Webster P.J., Wick G.A. & Zeng X. 2004. SEAFLUX. *Bulletin of the American Meteorological Society 85*, 409–424.

Curry J.A. & Webster P.J. 1999. Ocean surface exchanges of heat and fresh water. In J.R. Holton & P.J. Webster (eds.): *Thermodynamics of atmospheres and oceans*. Pp. 252–253. San Diego, CA: Academic Press.

da Silva A.M., Young C.C. & Levitus S. 1994. *Atlas of surface marine data 1994. vol. 1. Algorithms and procedures. NOAA Atlas NESDIS 6*. Washington, D.C.: U.S. Department of Commerce, National Oceanic and Atmospheric Administration,

National Environmental Satellite, Data, and Information Service.

Dawe J.T. & Thompson L. 2006. Effect of ocean surface currents on wind stress, heat flux, and wind power input to the ocean. *Geophysical Research Letters 33*, L09604, doi: 10.1029/2006GL025784.

ECMWF 1994. *The description of the ECMWF/WCRP Level III-A Global Atmospheric Data Archive*. Reading, MA: European Centre for Medium-Range Weather Forecasts Operations Department.

Fairall C.W., Bradley E.F., Hare J.E., Grachev A.A. & Edson J.B. 2003. Bulk parameterization of air–sea fluxes: update and verification for the COARE algorithm. *Journal of Climate 16*, 571–591.

Fairall C.W., Bradley E.F., Rogers D.P., Edson J.B. & Young G.S. 1996. Bulk parameterization of air–sea fluxes for Tropical Ocean–Global Atmosphere Coupled–Ocean Atmosphere Response Experiment. *Journal of Geophysical Research—Oceans 101*, 3747–3764.

Feng L. & Li J. 2006. A comparison of latent heat fluxes over global oceans for ERA and NCEP with GSSTF2. *Geophysical Research Letters 33*, L03810, doi: 10.1029/2005GL024677.

Ghil M. & Mo K.C. 1991. Interseasonal oscillation in the global atmosphere. Part II: Southern Hemisphere. *Journal of the Atmospheric Science 48*, 780–790.

Josey S.A. 2001. Comparison of ECMWF, NCEP–NCAR, and SOC surface heat fluxes with moored buoy measurements in the subduction region of the northeast Atlantic. *Journal of Climate 14*, 1780–1789.

Josey S.A., Kent E.C. & Taylor P.K. 1999. New insights into the ocean heat budget closure from analysis of the SOC air–sea flux climatology. *Journal of Climate 12*, 2856–2880.

Kalnay E., Kanamitsu M., Kistler R., Collins W., Deaven D., Gandin L., Iredell M., Saha S., White G., Woollen J., Zhu Y., Leetmaa A., Reynolds R., Chelliah M., Ebisuzaki W., Higgins W., Janowiak J., Mo K.C., Ropelewski C., Wang J., Jenne R. & Joseph D. 1996. The NCEP/NCAR 40-Year Reanalysis Project. *Bulletin of the American Meteorological Society 77*, 437–471

Kanamitsu M. 1989. Description of the NMC global data assimilation and forecast system. *Weather and Forecasting 4*, 335–342.

Kanamitsu M., Ebisuzaki W., Woolen J., Potter J. & Fiorino M. 2000. Overview of NCEP/DOE Reanalysis-2. *Proceedings of the Second WCRP International Conference on Reanalyses (Wokefield Park, nr. Reading, UK, 23–27 August 1999). WCRP-109. WMO/TD-985*. Pp. 1–4. Geneva: World Meteorological Organization.

Kanamitsu M., Ebisuzaki W., Woollen J., Yang S.-K., Hnilo J.J., Fiorino M. & Potter G.L. 2002. NCEP–DOE AMIP-II Reanalysis (R-2). *Bulletin of the American Meteorological Society 83*, 1631–1643.

King J.C. & Turner J. 1997. *Antarctic meteorology and climatology*. Cambridge: Cambridge University Press.

Klepp C., Andersson A. & Bakan S. 2008. The HOAPS climatology: evaluation of latent heat flux. *Flux News: Newsletter of the WCRP Working Group on Surface Fluxes 5*, 30–32.

Klinker E. 1997. Diagnosis of the ECMWF model performance over the tropical oceans. In: *Seminar proceedings on atmosphere–surface interaction*. Pp. 53–66. Reading: European Centre for Medium-Range Weather Forecasts.

Kondo J. 1975. Air–sea bulk transfer coefficients in diabatic conditions. *Boundary-Layer Meteorology 9*, 91–112.

Kubota M., Iwasaka N., Kizu S., Konda M. & Kutsuwada K. 2002. Japanese ocean flux data sets with use of remote sensing observations (J-OFURO). *Journal of Oceanography 58*, 213–225.

Kubota M., Kano A., Muramatsu H. & Tomita H. 2003. Intercomparison of various surface latent heat flux fields. *Journal of Climate 16*, 670–678.

Kubota M. & Tomita H. 2007. The present state of the J-OFURO air–sea interaction data product. *Flux News: Newsletter of the WCRP Working Group on Surface Fluxes 5*, 13–15.

Liu J. & Curry J.A. 2006. Variability of the tropical and subtropical ocean surface latent heat flux during 1989–2000. *Geophysical Research Letters 33*, L05706, doi: 10.1029/2005GL024809.

Li S.-M., Zhou M.-Y., Lu N.-P., Su L.-R., Wu M. L.C. &Wu Z.-M. 1997. 50°S 以南 海域的感热潜热通量的模式计算. (Model calculation of sensible and latent heat flux in the ocean area between 50°S and Antarctica.) *Acta Geophysica Sinica 40*, 460–467.

Moore G.W.K. & Renfrew I.A. 2002. An assessment of the surface turbulent heat fluxes from the NCEP–NCAR reanalysis over the Western Boundary Currents. *Journal of Climate 15*, 2020–2037.

Renfrew I.A., Moore G.W.K., Guest P.S. & Bumke K. 2002. A comparison of surface layer and surface turbulent flux observations over the Labrador Sea with ECMWF analyses and NCEP reanalyses. *Journal of Physical Oceanography 32*, 383–400.

Rouault M., Reason C.J.C., Lutjeharms J.R.E. & Beljaars A.C.M. 2003. Underestimation of latent and sensible heat fluxes above the Agulhas Current in NCEP and ECMWF analyses. *Journal of Climate 16*, 776–782.

Schlussel P., Schanz L. & Englisch G. 1995. Retrieval of latent heat flux and longwave irradiance at the sea-surface from SSM/I and AVHRR measurements. *Advances in Space Research 16*, 107–116.

Sen Gupta A. & England M.H. 2006. Coupled ocean–atmosphere–ice response to variations in the Southern Annular Mode. *Journal of Climate 19*, 4457–4486.

Siefridt L., Barnier B., Beranger K. & Roquet H. 1999. Evaluation of operational ECMWF surface heat fluxes: impact of parameterization changes during 1986–1996. *Journal of Marine Systems 19*, 113–135.

Sun B., Yu L. & Weller R.A. 2003. Comparisons of surface meteorology and turbulent heat fluxes over the Atlantic: NWP model analyses versus moored buoy observations. *Journal of Climate 16*, 679–695.

Tomita H., Kubota M., Cronin M.F., Iwasaki S., Konda M. &Ichikawa H. 2010. An assessment of surface heat fluxes

from J-OFURO2 at the KEO and JKEO sites. *Journal of Geophysical Research—Oceans 115*, C03018, doi: 10.1029/2009JC005545.

Thompson D. W. J., & Wallace J. M. 2000. Annular modes in the extratropical circulation. Part I: month-to-month variability. *Journal of Climate 13*, 1000–16.

Uppala S.M., Kållberg P.W., Simmons A.J., Andrae U., da Costa Bechtold V., Fiorino M., Gibson J.K., Haseler J., Hernandez A., Kelly G.A., Li X., Onogi K., Saarinen S., Sokka N., Allan R.P., Andersson E., Arpe K., Balmaseda M.A., Beljaars A.C.M., vande Berg L., Bidlot J., Bormann N., Caires S., Chevallier F., Dethof A., Dragosavac M., Fisher M., Fuentes M., Hagemann S., Hólm E., Hoskins B.J., Isaksen L., Janssen P.A.E.M., Jenne R., Mcnally A.P., Mahfouf J.-F., Morcrette J.-J., Rayner N.A., Saunders R.W., Simon P., Sterl A., Trenberth K.E., Untch A., Vasiljevic D., Viterbo P. & Woollen J. 2005. The ERA-40 re-analysis. *Quarterly Journal of the Royal Meteorological Society 131*, 2961–3012.

Wainer I., Taschetto A., Scoares J., De Oliveira A.P., Otto-Bliesner B. & Brady E. 2003. Intercomparison of heat fluxes in the South Atlantic. Part I: the seasonal cycle. *Journal of Climate 16*, 706–714.

Wang W. & McPhaden M.J. 2001. What is the mean seasonal cycle of surface heat flux in the equatorial Pacific? *Journal of Geophysical Research—Oceans 106*, 837–857.

Wentz F.J. 1994. *User's manual SSM/I-2 geophysical tapes. Technical Report 070194*. Santa Rosa, CA: Remote Sensing Systems.

Wentz F.J. 1997. A well-calibrated ocean algorithm for special sensor microwave/imager. *Journal of Geophysical Research—Oceans 102*, 8703–8718.

Yu L., Jin X. & Weller R.A. 2008. *Multidecade global flux datasets from the Objectively Analyzed Air–Sea Fluxes (OAFlux) Project: latent and sensible heat fluxes, ocean evaporation, and related surface meteorological variables*. Woods Hole, MA: Woods Hole Oceanographic Institution.

Yu L. & Weller R.A. 2007. Objectively analyzed air–sea heat fluxes for the global ocean-free oceans (1981–2005). *Bulletin of the American Meteorological Society 88*, 527–539.

Zeng X., Zhao M. & Dickinson R.E. 1998. Intercomparison of bulk aerodynamic algorithms for the computation of sea surface fluxes using TOGA COARE and TAO data. *Journal of Climate 11*, 2628—2644.